Journal of Experimental Botany, Vol. 71, No. 1 pp. 73–89, 2020
doi:10.1093/jxb/erz404 Advance Access Publication September 8, 2019
This paper is available online free of all access charges (see https://academic.oup.com/jxb/pages/openaccess for further details)

RESEARCH PAPER

Arabidopsis cargo receptor NBR1 mediates selective autophagy of defective proteins

Hyera Jung[1,*], Han Nim Lee[1,*,†], Richard S. Marshall[2,*], Aaron W. Lomax[3,‡], Min Ji Yoon[1,§], Jimi Kim[1], Jeong Hun Kim[1], Richard D. Vierstra[2,3,¶] and Taijoon Chung[1,¶]

[1] Department of Biological Sciences, Pusan National University, Busan, 46241, Republic of Korea
[2] Department of Biology, Washington University in St Louis, St Louis, MO 63130, USA
[3] Department of Genetics, University of Wisconsin, Madison, WI 53706, USA

[†] Present address: Department of Botany and Laboratory of Cell and Molecular Biology, University of Wisconsin, Madison, WI 53706, USA
[‡] Present address: Department of Soil Science, University of Wisconsin, Madison, WI 53706, USA
[§] Present address: Department of Life Sciences, College of Life Sciences and Biotechnology, Korea University, Seoul, 02841, Republic of Korea
* These authors contributed equally to this work.
¶ Correspondence: rdvierstra@wustl.edu or taijoon@pusan.ac.kr

Received 14 July 2019; Editorial decision 29 August 2019; Accepted 30 August 2019

Editor: Peter Bozhkov, Swedish University of Agricultural Sciences, Sweden

Abstract

Aggrephagy, a type of selective autophagy that sequesters protein aggregates for degradation in the vacuole, is an important protein quality control mechanism, particularly during cell stress. In mammalian cells, aggrephagy and several other forms of selective autophagy are mediated by dedicated cargo receptors such as NEIGHBOR OF BRCA1 (NBR1). Although plant NBR1 homologs have been linked to selective autophagy during biotic stress, it remains unclear how they impact selective autophagy under non-stressed and abiotic stress conditions. Through microscopic and biochemical analysis of *nbr1* mutants expressing autophagy markers and an aggregation-prone reporter, we tested the connection between NBR1 and aggrephagy in Arabidopsis. Although NBR1 is not essential for general autophagy, or for the selective clearance of peroxisomes, mitochondria, or the ER, we found that NBR1 is required for the heat-induced formation of autophagic vesicles. Moreover, cytoplasmic puncta containing aggregation-prone proteins, which were rarely observed in wild-type plants, were found to accumulate in *nbr1* mutants under both control and heat stress conditions. Given that NBR1 co-localizes with these cytoplasmic puncta, we propose that Arabidopsis NBR1 is a plant aggrephagy receptor essential for maintaining proteostasis under both heat stress and non-stress conditions.

Keywords: ATG8, autophagic flux, autophagosome, Floury2, protein misfolding, proteotoxic stress, ubiquitin.

Introduction

Autophagy is a trafficking route for directing cytoplasmic materials to the vacuole for degradation (Avin-Wittenberg *et al.*, 2018; Marshall and Vierstra, 2018*a*). In a major type of autophagy known as macroautophagy (hereafter referred to as autophagy), cargo is sequestered by a cup-shaped phagophore membrane that subsequently seals to form a double membrane-bound

Abbreviations: AIM, ATG8-interacting motif; ATG, autophagy-related; AZC, azetidine-2-carboxylic acid; ConA, concanamycin A; ER, endoplasmic reticulum; FL2, Floury2; GFP, green fluorescent protein; NBR1, NEIGHBOR OF BRCA1; PB1, Phox and Bem1p; PE, phosphatidylethanolamine; SP, signal peptide; UBA, ubiquitin-associated; WT, wild-type.

autophagosome. Autophagic cargo can include individual proteins, whole organelles, multi-subunit complexes, protein aggregates, and even invading pathogens residing in the cytoplasm, as well as material transported to the cytoplasm from other intracellular compartments. Autophagosomes then fuse with the tonoplast to deposit the internal vesicle, known as an autophagic body, and its contents into the vacuolar lumen for rapid breakdown by resident hydrolases.

Autophagy is driven by a conserved set of AUTOPHAGY-RELATED (ATG) proteins that regulate and execute the formation of autophagosomes and promote their delivery to the vacuole. At its nexus is the ubiquitin-fold protein ATG8, which becomes conjugated to the lipid phosphatidylethanolamine (PE) and hence localized on the cytosolic leaflet of autophagic membranes. Once integrated into the enveloping membranes, ATG8–PE acts as a docking platform to help tether appropriate cargo to the engulfing phagophore, and to promote autophagosome closure and fusion with vacuoles. These activities are mediated by a plethora of ATG8-binding adaptor and receptor proteins that bind ATG8–PE through either an ATG8-interacting motif (AIM; Pankiv *et al.*, 2007; Noda *et al.*, 2008) or an ATG8-binding ubiquitin-interacting motif (UIM; Marshall *et al.*, 2019) that docks into hydrophobic pockets on the surface of ATG8.

Autophagosomes capture their cargo either non-selectively or selectively. Whereas bulk non-selective autophagy is typically induced by starvation and plays a role in nutrient recycling, selective autophagy is driven by receptors with affinity for both the cargo and ATG8 (Marshall and Vierstra, 2018*a*). Examples of selective autophagy include aggrephagy, which clears protein aggregates; mitophagy, pexophagy, reticulophagy, proteaphagy, and ribophagy, which recycle mitochondria, peroxisomes, the ER, proteasomes, and ribosomes, respectively; and xenophagy, which eliminates invading pathogens (Liu *et al.*, 2012; Kim *et al.*, 2013*b*; Shibata *et al.*, 2013; Li *et al.*, 2014; Marshall *et al.*, 2015; Hafrén *et al.*, 2017; Haxim *et al.*, 2017; Marshall and Vierstra, 2018*a*). Cargo is often first tagged with ubiquitin, which enables recognition by a family of autophagy receptors with affinity for both ubiquitin and ATG8.

Aggrephagy is part of a concerted effort to maintain protein homeostasis, especially under conditions that elicit proteotoxic stress. Under such stress, cells attempt to (i) refold misfolded proteins using a suite of dedicated chaperones, (ii) degrade them via the ubiquitin–proteasome system, and/or (iii) sequester them away from the rest of the cytoplasm through aggregation. Once aggregated, additional attempts at refolding are possible or, if all attempts fail, these potentially cytotoxic aggregates are removed through aggrephagy (Harper and Bennett, 2016; Yoon and Chung, 2019). The p62 receptor (also known as sequestosome-1) is a major effector of aggrephagy in mammalian cells. In this capacity, p62 coalesces its targets through head-to-tail multimerization using its N-terminal Phox and Bem1p (PB1) domains to generate long polymers that can concentrate the aggregated targets (Wurzer *et al.*, 2015). Target binding often occurs through interactions between the ubiquitin-associated (UBA) domain in p62 and ubiquitin moieties conjugated to the misfolded species, while tethering of the aggregates to ATG8 occurs via an embedded AIM (Bjørkøy *et al.*, 2005; Komatsu *et al.*, 2007; Pankiv *et al.*, 2007). Many metazoan species also employ NEIGHBOR OF BRCA1 (NBR1) for aggrephagy, whose domain organization is very similar to that of p62, while other eukaryotes, including plants, appear to rely solely on NBR1-type receptors for removing protein aggregates (Svenning *et al.*, 2011).

Currently, the functions of the plant NBR1 homologs remain unclear. A conserved role in selective autophagy was suggested based on their similar domain organization, ability to bind ubiquitin and ATG8 *in vitro*, and a subcellular localization like those of mammalian NBR1 and p62 (Svenning *et al.*, 2011; Zientara-Rytter *et al.*, 2011, 2014). For example, NBR1 fused to fluorescent reporters accretes in cytoplasmic aggregates that appear to be directed to the vacuole via a pathway dependent on the PB1 and UBA domains, and the core autophagy machinery (Svenning *et al.*, 2011). As expected for an aggrephagy receptor, Arabidopsis *nbr1* mutants are hypersensitive to various abiotic stresses and overaccumulate insoluble protein aggregates during heat stress (Zhou *et al.*, 2013). NBR1 also contributes to plant immunity in Arabidopsis by binding to specific viral components and mediating their selective clearance (Hafrén *et al.*, 2017, 2018), and possibly by promoting selective autophagy of unknown bacterial proteins (Üstün *et al.*, 2018). In tobacco, NBR1 was shown to play a role in anti-fungal defense (Dagdas *et al.*, 2016) and localized to sites of host–pathogen interactions (Dagdas *et al.*, 2018).

It is also unclear which conditions promote aggrephagy in plant cells. Heat shock was proposed to induce autophagy, which then targets heat-denatured protein aggregates for degradation (Avin-Wittenberg, 2019). This is based on the observation that autophagic vesicles accumulate in Arabidopsis cells exposed to heat shock (Zhou *et al.*, 2013; Yang *et al.*, 2016). However, autophagic vesicles can also hyper-accumulate when the biogenesis and turnover of autophagosomes are interrupted at any step after phagophore nucleation (Mizushima *et al.*, 2010; Kang *et al.*, 2018), thus raising the possibility that heat shock actually suppresses autophagy.

In this study, we discovered that bulk autophagy is impaired by prolonged heat and protein folding stress. We further examined the dynamics and localization of NBR1 in Arabidopsis and its ability to clear a protein designed to be aggregation-prone, which collectively demonstrated that NBR1 acts as a bona fide aggrephagy receptor responsible for protein quality control under both heat stress and non-stress conditions. In this capacity, we propose that NBR1 promotes the formation of protein aggregates and helps clear aggregation-prone cargo destined for autophagy.

Materials and methods

Plant materials and growth conditions

All Arabidopsis plants were the Columbia (Col-0) ecotype. The *nbr1-1* (SALK_135513), *nbr1-2* (GABI_246H08), *nbr1-3* (SALK_144852), and *nbr1-4* (WiscDsLoxHs007_07A) alleles were obtained from the Arabidopsis Biological Resource Center (ABRC). All insertion mutants were confirmed by genomic PCR using 5′ and 3′ gene-specific primers (LP and RP, respectively) in conjunction with an appropriate T-DNA left border-specific primer (BP; Supplementary Table S1 at *JXB* online).

The Arabidopsis *atg7-2* mutant (Chung *et al.*, 2010) and transgenic plants expressing *ProUBQ10:GFP-ATG8A* (Kim *et al.*, 2013*b*) were as previously described. The *ProUBQ10:mCherry-NBR1*, *ProSSU:FL2-GFP*, and *Pro35S:GFP-FL2ΔSP* reporters were introduced into the *Agrobacterium tumefaciens* strain GV3101 and transformed into Arabidopsis by the floral dip method (Clough and Bent, 1998).

Surface-sterilized seeds were germinated in 1 ml of liquid Murashige and Skoog (MS) medium with 1% (w/v) sucrose. Seedlings were incubated in the medium with gentle shaking (100 rpm) at 21–23 °C under a long-day photoperiod (16 h light/8 h darkness). When necessary, stock solutions of DMSO, (*N*-benzyloxycarbonyl)-leucinyl-leucinyl-leucinal (MG132; Sigma-Aldrich, St Louis, MO, USA), azetidine-2-carboxylic acid (AZC; Santa Cruz Biotechnology, Dallas, TX, USA), or concanamycin A (ConA; Cayman Chemical, Ann Arbor, MI, USA) were added to the liquid medium. Heat shock was applied by placing the microtiter plates containing the hydroponic culture of Arabidopsis seedlings into a water bath set to 22, 37, or 45 °C.

Recombinant DNA constructs

To prepare the pMDC99-ProUBQ10:mCherry-NBR1 reporter expressing mCherry fused to NBR1 from the Arabidopsis *UBQ10* promoter, an entry clone containing the full-length *NBR1* cDNA was obtained from the ABRC (clone ID: G25119) and recombined into the destination vector pMDC99-ProUBQ10:mCherry (Suttangkakul *et al.*, 2011) via the LR clonase II reaction (Thermo Fisher Scientific, Waltham, MA, USA).

To prepare pMDC107-ProSSU:FL2-GFP expressing FLOURY2 (FL2) fused to green fluorescent protein (GFP), a 1726-bp promoter sequence from the Arabidopsis Rubisco small subunit gene *RBCS1A* was amplified using primers AtSSUp_F1AscI and AtSSUp_R2AscI (Supplementary Table S1) from Arabidopsis Col-0 genomic DNA. The amplified DNA fragment was then cloned into the pGEM-T Easy vector (Promega, Madison, WI, USA), digested with *Sac*II, and the resulting fragment was converted to blunt ends with Klenow polymerase and then further digested with *Pst*I. The resulting fragment was then ligated into pMDC107 (Curtis and Grossniklaus, 2003) after its *Xba*I site was converted to blunt ends with Klenow polymerase and digested with *Sbf*I, to generate the destination vector pMDC107-ProSSU. The *Floury2* (*FL2*) cDNA was amplified from total RNA isolated from the maize (*Zea mays*) B73 inbred line by RT-PCR, using primers FL2_F1 and FL2_R2(xG) (Supplementary Table S1). The *FL2* cDNA was cloned into pENTR/D-TOPO (Thermo Fisher Scientific) to produce pENTR/D-TOPO-FL2, which was then recombined into pMDC107-ProSSU via the LR clonase II reaction.

To generate pMDC43-FL2ΔSP expressing GFP fused to FL2 lacking its N-terminal signal peptide (SP) from the cauliflower mosaic virus *35S* promoter, the coding sequence of *FL2ΔSP* was amplified using primers FL2_F3cacc and FL2_R2 (Supplementary Table S1), with pENTR/D-TOPO-FL2 as the template. The amplified DNA fragment was then cloned into pENTR/D-TOPO to produce pENTR/D-TOPO-FL2ΔSP, which was then recombined into pMDC43 (Curtis and Grossniklaus, 2003) via the LR clonase II reaction.

Generation of anti-NBR1 antibody

The coding region encompassing the N-terminal portion of NBR1 (residues 1–376) was PCR amplified from Arabidopsis Col-0 cDNA and recombined sequentially into the pDONR221 plasmid via the BP clonase II reaction (Thermo Fisher Scientific), followed by the pDEST17 plasmid via the LR clonase II reaction, which resulted in the appendage of codons for an N-terminal 6His tag. The protein was then recombinantly expressed in *Escherichia coli* strain BL21(DE3) by a 4-h induction with 1 mM isopropyl β-D-1-thiogalactopyranoside. Cells were harvested, frozen in liquid nitrogen, and lysed in Bug-Buster Master Mix (Sigma-Aldrich). The insoluble fraction was extracted with 6 M urea and the solubilized 6His–NBR1 fragment was purified under denaturing conditions with nickel–nitrilotriacetic acid agarose beads (Thermo Fisher Scientific). The resulting 6His–NBR1 fragment was then subjected to SDS-PAGE, and the gel was stained with Coomassie Brilliant Blue. The protein band was extracted from the gel with 1% SDS and injected directly into rabbits.

Immunoblot analysis

Total protein extracts were prepared by homogenizing Arabidopsis seedlings in Laemmli sample buffer containing 10% (v/v) 2-mercaptoethanol, followed by clarification at 16 000 *g* for 10 min. Alternatively, samples were homogenized in protein extraction buffer (50 mM Tris–HCl (pH 7.5),150 mM NaCl, 1 mM phenylmethylsulfonyl fluoride, 1× plant protease inhibitor cocktail, 50 μM MG132, 2 mM dithiothreitol), clarified at 16 000 *g* for 5 min at 4 °C, and the supernatant then mixed with 0.25 volumes of 5× SDS-PAGE sample buffer containing 10% (v/v) 2-mercaptoethanol. Protein extracts were heated to 95 °C, separated by SDS-PAGE, and transferred onto polyvinylidene difluoride membranes (MilliporeSigma, Burlington, MA, USA). Primary and secondary antibodies were diluted in 1× phosphate buffered saline (PBS) with 0.1% (v/v) Triton X-100 (PBS-T) containing 5% (w/v) non-fat dry milk, and secondary antibodies were diluted in 1× PBS-T. Alternatively, primary and secondary antibodies were diluted in 1× PBS containing 1% (w/v) non-fat dry milk. Antibodies against GFP (Sigma-Aldrich), catalase (Agrisera, Vännäs, Sweden), voltage-dependent anion channel 1 (VDAC1; Agrisera), ATG8 (Abcam, Cambridge, MA, USA), UDP-glucose pyrophosphorylase (UGPase, Agrisera), and histone H3 (Abcam) were obtained from the indicated sources. Quantification of band intensities was performed using either ImageJ (National Institutes of Health, Bethesda, MD, USA) or TotalLab software (Non-linear Dynamics, Newcastle upon Tyne, UK).

Quantitative real-time PCR analysis

For quantitative real-time (qRT)-PCR, total RNA was extracted from 9-day-old seedlings with Trisure (Bioline, London, UK), and then treated with DNase I according to the manufacturer's instructions. The cDNA was synthesized using RevertAid H Minus reverse transcriptase (Thermo Fisher Scientific) and oligo$(dT)_{20}$ primers. qRT-PCR was performed using EvaGreen (SolGent, Daejeon, Korea), and the relative transcript abundance of target genes was calculated by the $\Delta\Delta C_T$ method (Livak and Schmittgen, 2001), using the *ACT2* cDNA as an internal control (Gladman *et al.*, 2016). All primer sequences are provided in Supplementary Table S1.

Confocal microscopy and image processing

Fluorescence images were acquired using the confocal laser scanning microscopes LSM510 and LSM800 (Carl Zeiss) at Pusan National University. For LSM510, a 488 nm laser and 500–530 nm infra-red band-pass emission filters were used for GFP, and a 543 nm laser and 565–615 nm infra-red band-pass emission filters were used for mCherry. For LSM800, a 488 nm diode laser was used for GFP detection. The Analyze Particles function in ImageJ was used to identify and quantify puncta. Autophagic body-type distributions of GFP–FL2ΔSP and GFP–ATG8A puncta were verified by a Z-stack series of 1 μm optical sections from ConA-treated samples.

Accession numbers

Sequence data from this article can be found in the National Center for Biotechnology Information (http://www.ncbi.nlm.nih.gov/) or the Arabidopsis Information Resource (http://www.arabidopsis.org/) databases under the following identifiers: ACT2, At3g18780; ATG7, At5g45900; ATG8A, At4g21980; $FL2^{B73}$, NP_001105057; HSFA7A, At3g51910; HSP90, At5g52640; NBR1, At4g24690; PAA2, At2g05840; and RBC1S1A, At1g67090.

Results

Autophagy is impaired by prolonged heat and folding stress

To investigate aggrephagy in plant cells, we examined a number of conditions that might trigger protein misfolding/unfolding

as a way to hyper-accumulate protein aggregates *in planta*, which could then be substrates of NBR1-mediated autophagy. One obvious candidate was heat shock, which readily causes protein misfolding and aggregation in a variety of cellular systems (Mogk *et al.*, 2018; McLoughlin *et al.*, 2019). However, it was unclear how effective heat shock would be as a strategy for studying aggrephagy, as severe heat shock might damage the autophagic machinery. As such, we first employed three separate methods to monitor autophagic flux and determine how heat stress influences autophagy (Mizushima *et al.*, 2010).

First, we inquired whether autophagic bodies could be detected in root cells that were exposed to a 37 °C heat shock. For this purpose, we used a transgenic line expressing GFP–ATG8A from the constitutive *UBQ10* promoter (*ProUBQ10:GFP-ATG8A*) as an autophagic vesicle marker (Kim *et al.*, 2013*b*), and treated the seedlings with ConA, which stabilizes autophagic bodies and thus enhances their detection (Yoshimoto *et al.*, 2004; Thompson *et al.*, 2005). As expected, autophagic bodies labeled with GFP–ATG8A became evident in the vacuoles of root cells treated with ConA at normal temperatures (Fig. 1A; WT, 22 °C, + ConA), consistent with previous reports of basal autophagy in Arabidopsis (Yoshimoto *et al.*, 2004; Thompson *et al.*, 2005; Sláviková *et al.*, 2005). A comparable accumulation was also seen in wild-type (WT) root cells exposed to 37 °C for 8 h and subsequently allowed to recover at 22 °C for an additional hour (Fig. 1A; WT, 37 °C, + ConA), but not in

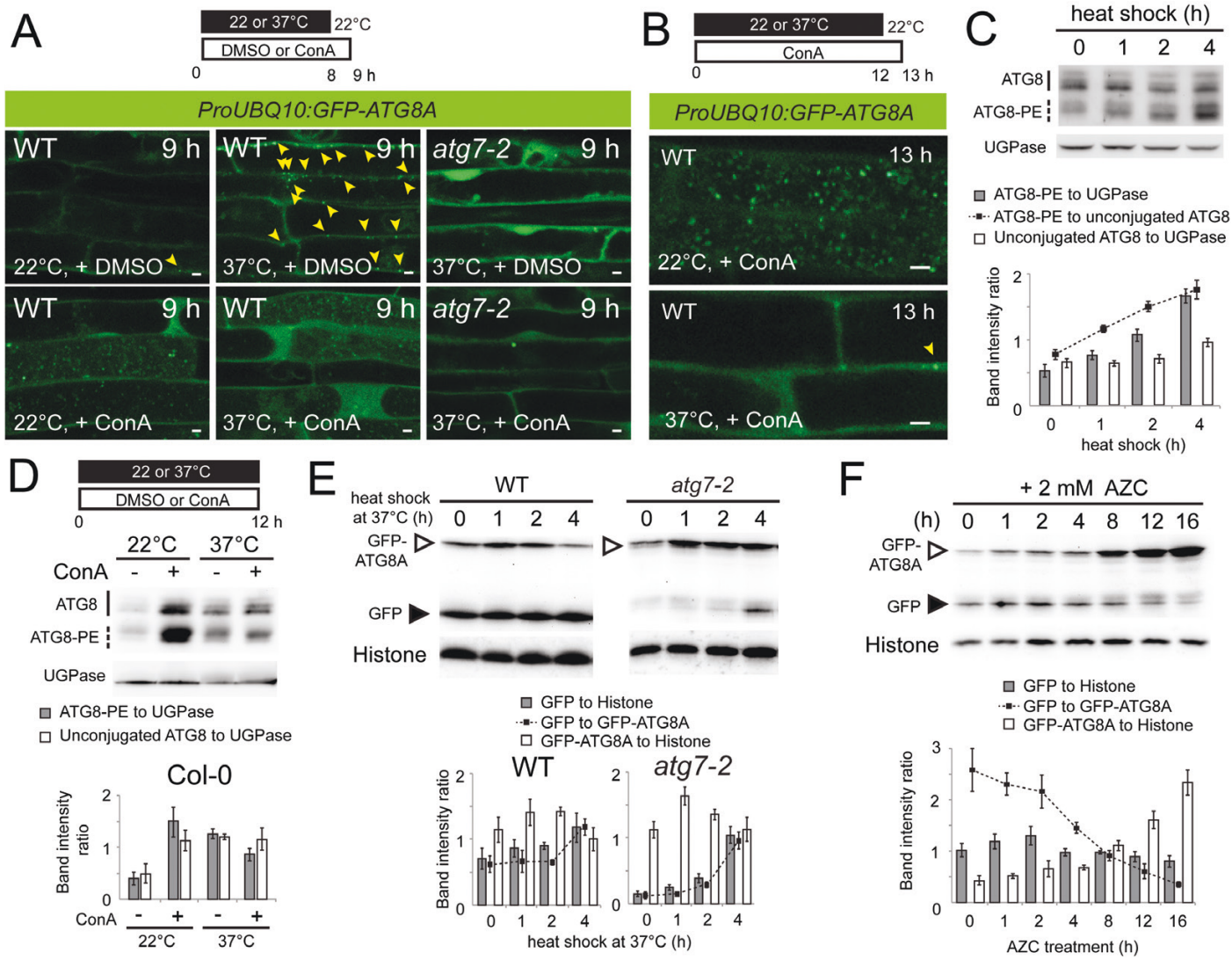

Fig. 1. Autophagic flux is inhibited during prolonged heat stress. (A, B) Confocal images of wild-type (WT) or *atg7-2* root cells expressing *GFP-ATG8A*. Nine-day-old seedlings were incubated at 22 or 37 °C in liquid MS medium containing DMSO or 0.5 μM ConA for 8 h (A) or 12 h (B), and recovered at 22 °C for 0.5–1 h prior to observation. Scale bars: 5 μm. (C) Immunoblot analysis with anti-ATG8 antibodies showing endogenous ATG8 levels in 9-day-old WT seedlings exposed to 37 °C heat shock for the indicated time periods. (D) Immunoblot showing endogenous ATG8 levels in 9-day-old WT seedlings that were incubated for 12 h at control (22 °C) or heat shock (37 °C) temperatures in liquid medium containing DMSO or 0.5 μM ConA. (E) GFP–ATG8A cleavage assays of heat-exposed WT and *atg7-2* seedlings expressing *GFP-ATG8A*. Protein extracts were prepared from 9-day-old seedlings exposed to 37 °C heat shock for the indicated time periods and subjected to immunoblot analysis with anti-GFP antibodies. (F) GFP–ATG8A cleavage assay of plants exposed to 2 mM AZC for the indicated time periods. Graphs below (C–F) show quantification of band intensity ratios (mean ±SE; *n*=4 seedling populations). For the anti-ATG8 immunoblots (C, D), unconjugated and lipidated ATG8 proteins are marked by solid and dashed lines, respectively. In the anti-GFP immunoblots (E, F), full-length GFP–ATG8A and the free GFP cleavage product are indicated by open and solid arrowheads, respectively. The anti-UDP-glucose pyrophosphorylase (UGPase; C, D) and anti-histone H3 (E, F) immunoblots were used to confirm near equal protein loading.

similarly treated *atg7-2* root cells, which lack the E1 activating enzyme essential for ATG8 lipidation and ATG8-mediated autophagy (Chung *et al.*, 2010; Fig. 1A; *atg7-2*, 37 °C, + ConA). Conversely, root cells exposed to the 37 °C heat stress for 12 h and allowed to recover for an additional hour did not accumulate autophagic bodies (Fig. 1B), implying that longer exposure to 37 °C inhibits autophagy. Without ConA treatment, cytoplasmic puncta decorated with GFP–ATG8A were occasionally observed in control cells (Fig. 1A; WT, 22 °C, +DMSO; indicated by an arrowhead) but their abundance increased substantially in heat-exposed cells (Fig. 1A; WT, 37 °C, + DMSO), as previously observed with Arabidopsis cells exposed to 42 °C (Yang *et al.*, 2016) or 45 °C (Zhou *et al.*, 2013).

Next, we examined the effect of heat shock on endogenous ATG8 levels by immunoblot analysis of WT seedling extracts with anti-ATG8 antibodies. Exposure to 37 °C increased the level of the ATG8–PE adduct relative to the free form (Fig. 1C), suggesting that ATG8 lipidation is activated by a mild heat shock. However, higher ATG8–PE levels in heat-exposed seedlings could also arise if autophagy was partially blocked by heat, thus interfering with its autophagic turnover. To test this possibility, we combined heat shock with ConA treatment. If heat shock induced autophagy, ConA treatment combined with heat shock should further stabilize ATG8–PE in the vacuole, but if the heat shock interfered with autophagosome dynamics in the cytoplasm, ConA impact on ATG8–PE levels should be negligible. Here, we found that stabilization of ATG8–PE by ConA was evident in control seedlings but minimal in seedlings exposed to a 12-h heat shock (Fig. 1D). This implies that the higher level of ATG8–PE seen in seedlings exposed to prolonged heat stress (Fig. 1C) was partly due to impaired autophagic flux.

A drawback of measuring autophagic flux using ConA is that it fails to detect a rapid induction of autophagy, because stabilization of both autophagic bodies and ATG8–PE requires incubation times sufficiently long for the vacuolar pH to increase. Consequently, to measure autophagic flux during early responses to heat shock, we exploited the GFP–ATG8 cleavage assay based on the *GFP-ATG8A* reporter. This assay exploits the fact that GFP–ATG8A, once deposited into the vacuole, is degraded by resident proteases to release a relatively stable free GFP moiety, which can be readily quantified by immunoblot analysis with anti-GFP antibodies following SDS-PAGE of total seedling extracts (Chung *et al.*, 2010; Shin *et al.*, 2014; Suttangkakul *et al.*, 2011). Autophagic flux can then be estimated by comparing the amount of the free GFP relative to that of the GFP–ATG8A fusion (Marshall *et al.*, 2015; Kang *et al.*, 2018). Using this cleavage assay, we found that a 37 °C heat shock did not alter autophagic flux, based on a stable ratio of GFP to GFP–ATG8A over a 2-h heat shock at 37 °C (Fig. 1E). Although the ratio slightly increased by 4 h of heat shock, a similar increase was observed in the *atg7-2* background, which could reflect instability of the GFP–ATG8A reporter during prolonged high temperatures (Fig. 1E).

To confirm the inhibitory effect of extended heat stress on autophagic flux, we inquired whether heat shock would impact starvation-induced autophagy caused by the lack of nitrogen (Suttangkakul *et al.*, 2011). While autophagic flux induced by nitrogen deficiency was not impacted by a 2-h heat shock at 37 °C, it was suppressed by a 12-h exposure (Supplementary Fig. S1). Collectively, the data imply that autophagic flux is not greatly impacted by a short (1–2 h) exposure to 37 °C heat stress, but is gradually suppressed by prolonged exposure.

We also tested whether amino acid analogs that cause protein misfolding also induced autophagy, in this case by treating Arabidopsis seedlings with the proline analog AZC, whose incorporation into nascent polypeptides instead of proline distorts protein secondary structure (Trotter *et al.*, 2002; Duttler *et al.*, 2013; Wang *et al.*, 2013). Autophagic flux was not influenced by a short exposure to AZC but, unexpectedly, was strongly inhibited after 8 h of AZC treatment, as judged by a persistent decrease in the relative ratio of GFP to GFP–ATG8A (Fig. 1F). Taken together, we concluded that general autophagic flux is not significantly altered by short exposures to heat shock (up to 4 h) or folding stress (up to 2 h), but is suppressed by longer exposures. Consequently, we considered it best to use shorter treatments with heat shock or amino acid analogs to induce proteotoxic stress when studying their effects on autophagy.

Arabidopsis nbr1-2 *and* nbr1-4 *mutants do not accumulate NBR1 proteins*

To examine the roles of Arabidopsis *NBR1* during proteotoxic stress, we identified a collection of homozygous *nbr1* mutant lines with potentially compromised expression. In addition to the previously described *nbr1-2* (Zhou *et al.*, 2013) and *nbr1-4* (Young *et al.*, 2019) alleles, we describe here *nbr1-3*, which harbors a T-DNA insertion within the third intron (Fig. 2A). The *nbr1-2* allele fails to express detectable levels of the *NBR1* transcript and is considered a strong, if not null, allele (Zhou *et al.*, 2013). RT-PCR analyses conducted here showed that homozygous *nbr1-3* plants express much reduced levels of the full-length transcript and thus might represent a weak allele, whereas the homozygous *nbr1-4* plants failed to express the full-length transcript and thus might also be a strong, if not null, allele (Fig. 2B, C).

Previous studies reported that WT plants accumulate very low levels of NBR1 protein under non-stressed conditions, whereas strong autophagy mutants hyper-accumulate the NBR1 polypeptide, as expected if it were degraded along with its substrates by autophagy (Svenning *et al.*, 2011). Here, we similarly observed a hyper-accumulation of NBR1 in *atg7-2* seedlings (Fig. 2D). Two species were detected: one at ~70 kDa that likely represents the actual NBR1 polypeptide based on its calculated mass of 76 kDa, and another at ~100 kDa that possibly represents a post-translationally modified form (see Discussion). That both species were generated from the *NBR1* locus was supported by their absence or reduced accumulation in the three *nbr1* lines (Fig. 2D). When the *atg7-2* mutant was crossed with the *nbr1* alleles, the resulting *atg7-2 nbr1-2* and *atg7-2 nbr1-4* double mutants also failed to accumulate the ~70 and ~100 kDa NBR1 bands, whereas small amounts accumulated in the *atg7-2 nbr1-3* double mutant (Fig. 2D), thus confirming that the *nbr1-2* and *nbr1-4* mutants are null for the NBR1 protein while the *nbr1-3* mutant represents a weaker knock-down allele (Fig. 2D).

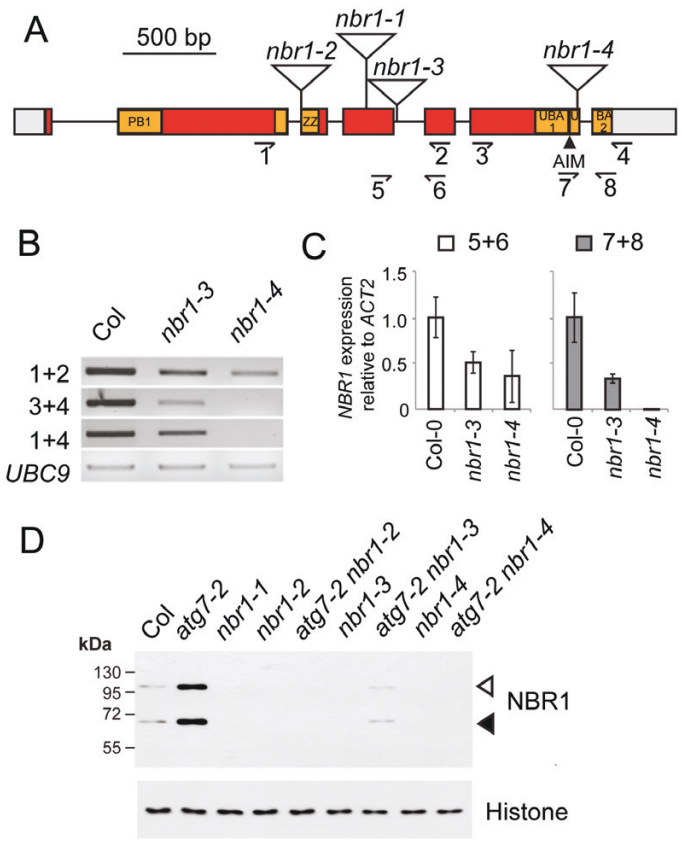

Fig. 2. Molecular characterization of Arabidopsis *nbr1* mutants. (A) Diagram of the Arabidopsis *NBR1* gene. The coding region is illustrated by colored boxes (exons) connected by lines (introns), whereas grey boxes correspond to untranslated regions. Domains of interest (Svenning *et al.*, 2011) are highlighted in orange: PB1, Phox and Bem1p domain; ZZ, ZZ-type zinc finger domain; UBA1 and UBA2, two ubiquitin-associated domains; AIM, ATG8-interacting motif. The positions of T-DNA insertions are indicated by open triangles. The positions of primers used for RT-PCR analysis in (B, C) are indicated by half-arrows. (B, C) RT-PCR verifies the impact of the new *nbr1* alleles on *NBR1* transcript abundance. For qRT-PCR assays (C), the relative expression of *NBR1* was calculated using *ACTIN 2* (*ACT2*) as a reference transcript. Each column represents the mean ±SE; *n*=3 seedling populations. (D) Representative image of immunoblot analysis with anti-NBR1 antibodies to determine NBR1 protein levels in wild-type (WT), *atg7*, *nbr1*, and their double mutant combinations. Each lane contains crude protein extract prepared from seedlings of the indicated genotype grown in liquid medium for 7 d. Solid and open arrowheads indicate the 70-kDa and 100-kDa NBR1 bands, respectively. The molecular masses indicated on the left are estimated from protein size markers. The anti-histone H3 immunoblot was used to confirm near equal protein loading.

Bulk autophagy is functional but aggregate formation is impaired in nbr1 *mutants*

Previous studies showed that *nbr1* mutants lacked two phenotypes common for mutants affecting the core autophagy machinery, namely accelerated leaf senescence and hypersensitivity to fixed-carbon starvation (Zhou *et al.*, 2013; Hafrén *et al.*, 2017), suggesting that general autophagy occurs normally in these backgrounds. Still, it was unclear whether autophagic flux would be altered and how *NBR1* would interact genetically with *ATG7*. To measure autophagic flux in the *nbr1* single and *nbr1 atg7* double mutants, we crossed the *nbr1-2* and *nbr1-4* alleles with an *atg7-2* line expressing the *ProUBQ10:GFP-ATG8A* reporter (Shin *et al.*, 2014), and obtained *nbr1* single and *nbr1 atg7* double homozygous combinations expressing the reporter in the F_2 generation. Assays for GFP–ATG8A cleavage with these lines showed that autophagic flux was robust and comparable to WT in the *nbr1* single mutants, but was absent in the *nbr1 atg7* double mutants, as in the *atg7-2* mutant alone (Fig. 3A), demonstrating that overall flux is not significantly altered by removing NBR1. In addition, *nbr1-2* seedlings treated with ConA accumulated normal levels of autophagic bodies (Supplementary Fig. S2A, +ConA), confirming that bulk autophagy remained active. Treatment of *nbr1-2* seedlings with AZC for 2 h also did not lead to a significant increase in the abundance of cytoplasmic GFP–ATG8A puncta (Supplementary Fig. S2B, C). Likewise, the GFP–ATG8A cleavage assay indicated that autophagic flux in AZC-treated WT and *nbr1-2* mutant seedlings was indistinguishable from their DMSO-treated controls (Supplementary Fig. S2D).

Next, we analysed the dynamics of GFP–ATG8A in WT and *nbr1* cells upon heat shock. While root cells kept at 22 °C retained a diffuse distribution of the reporter, numerous cytoplasmic puncta of various sizes appeared after exposure to 37 °C for 4 h, some of which presumably represented autophagic structures (phagophores or autophagosomes; indicated by arrowheads in Fig. 3B, C). However, when we similarly analysed the response of the *atg7-2* mutant, these structures were still evident, though the population shifted to consist mostly of larger puncta, with much fewer of the smaller puncta present (Fig. 3B, D). These larger puncta (indicated by arrows in Fig. 3B) could also be seen in non-stressed cells, suggesting that a block in autophagy enhanced their accumulation. As the lack of ATG7 should block synthesis of ATG8–PE and subsequent assembly of autophagic vesicles (Chung *et al.*, 2010; Kang *et al.*, 2018), we were left to conclude that these large foci represent another cellular structure that is able to coalesce non-lipidated ATG8.

One obvious possibility is that these large cytoplasmic foci represent protein aggregates awaiting autophagy. In fact, Yoshimoto *et al.* (2004) observed similarly large and bright GFP–ATG8a foci in mutants missing ATG4a/b, and proposed that these large puncta do not represent autophagic vesicles but are instead protein aggregates. Given that such aggregates might also contain NBR1, we tested whether the abundance of these structures was altered in an *nbr1* mutant. Elimination of NBR1 via the *nbr1-2* (Fig. 3B, C) or *nbr1-4* (Fig. 3C; Supplementary Fig. S3) alleles greatly reduced the appearance of these larger cytoplasmic structures after heat stress, with or without the *atg7-2* mutation. The structures could again be seen when we rescued *nbr1-2* roots with an mCherry–NBR1 reporter, indicating that NBR1 promoted the development of these structures and/or their association with ATG8, presumably through its ability to bind ATG8 via its AIM.

Heat stress promotes the association of NBR1 and ATG8 with cytoplasmic aggregates

To further test the relationship between NBR1 and the aggregates formed after heat shock, we followed by confocal

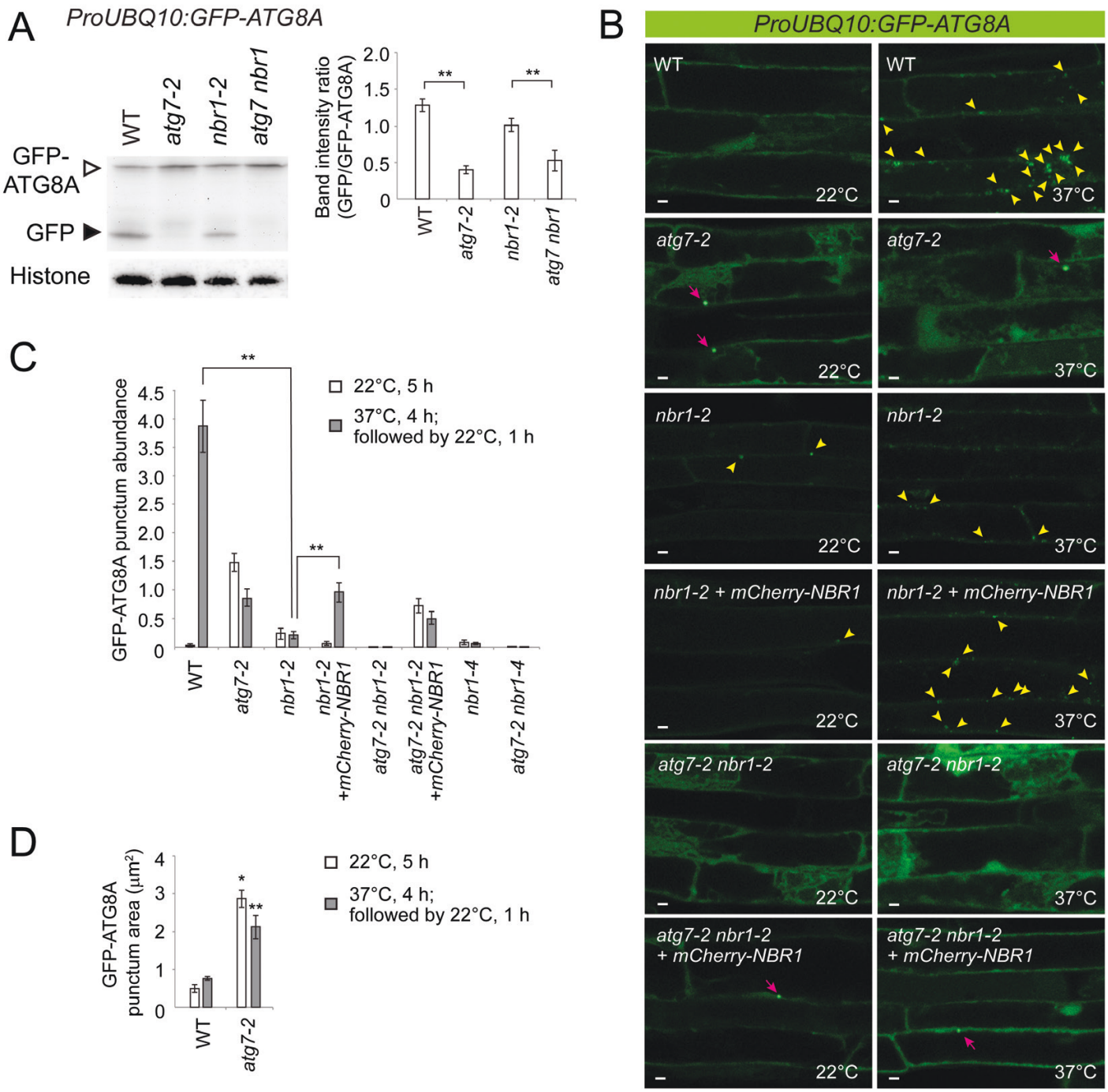

Fig. 3. NBR1 is not essential for bulk autophagy but promotes the formation of autophagic vesicles during heat stress. (A) GFP–ATG8A cleavage assay to assess autophagic flux in wild-type (WT), *atg7-2*, *nbr1-2*, and *atg7-2 nbr1-2* double mutant plants. Protein extracts were prepared from seedlings of the indicated genotypes, which were grown in liquid medium for 9 d. Each column represents the mean ±SE; *n*=4 seedling populations. The anti-histone H3 immunoblot was used to confirm near equal protein loading. (B) Confocal images of mature root cells expressing *GFP-ATG8A* in the genetic background of WT, *atg7-2*, *nbr1-2*, or *atg7-2 nbr1-2* double mutants, plus *nbr1-2* and *atg7-2 nbr1-2* co-expressing *mCherry-NBR1* as a complementation construct. The images were acquired from 9-day-old seedlings that were placed at 22 °C (left panels) or 37 °C (right) for 4 h and subsequently recovered at 22 °C for 0.5 to 1 h prior to observation. Yellow arrowheads and magenta arrows indicate GFP–ATG8A puncta with an approximate diameter of <1 μm and >1 μm, respectively. Scale bars: 5 μm. (C, D) Quantification of GFP–ATG8A punctum abundance (C) (number of puncta per 10 000 μm^2) and dimension (D) in multiple images represented by those shown in (B) and Supplementary Fig. S3. Each column represents the mean ±SE; *n*=48–83 images (C) or 2–71 puncta (D) per sample. Columns marked with asterisks represent treatments or mutants that were significantly different from the control treatment or WT, according to two-way (genotype 1×genotype 2, or genotype×treatment) ANOVA followed by Tukey's *post hoc* test. **P*<0.05; ***P*<0.01.

fluorescence microscopy mCherry–NBR1 in WT and *atg7-2* seedlings (Fig. 4A). In the WT background, little to no mCherry–NBR1 signal was evident both at 22 °C and after a 4-h exposure to 37 °C, consistent with its rapid turnover by autophagy (Fig. 4A). However, when the reporter was introgressed into the *atg7-2* mutant, strong mCherry–NBR1

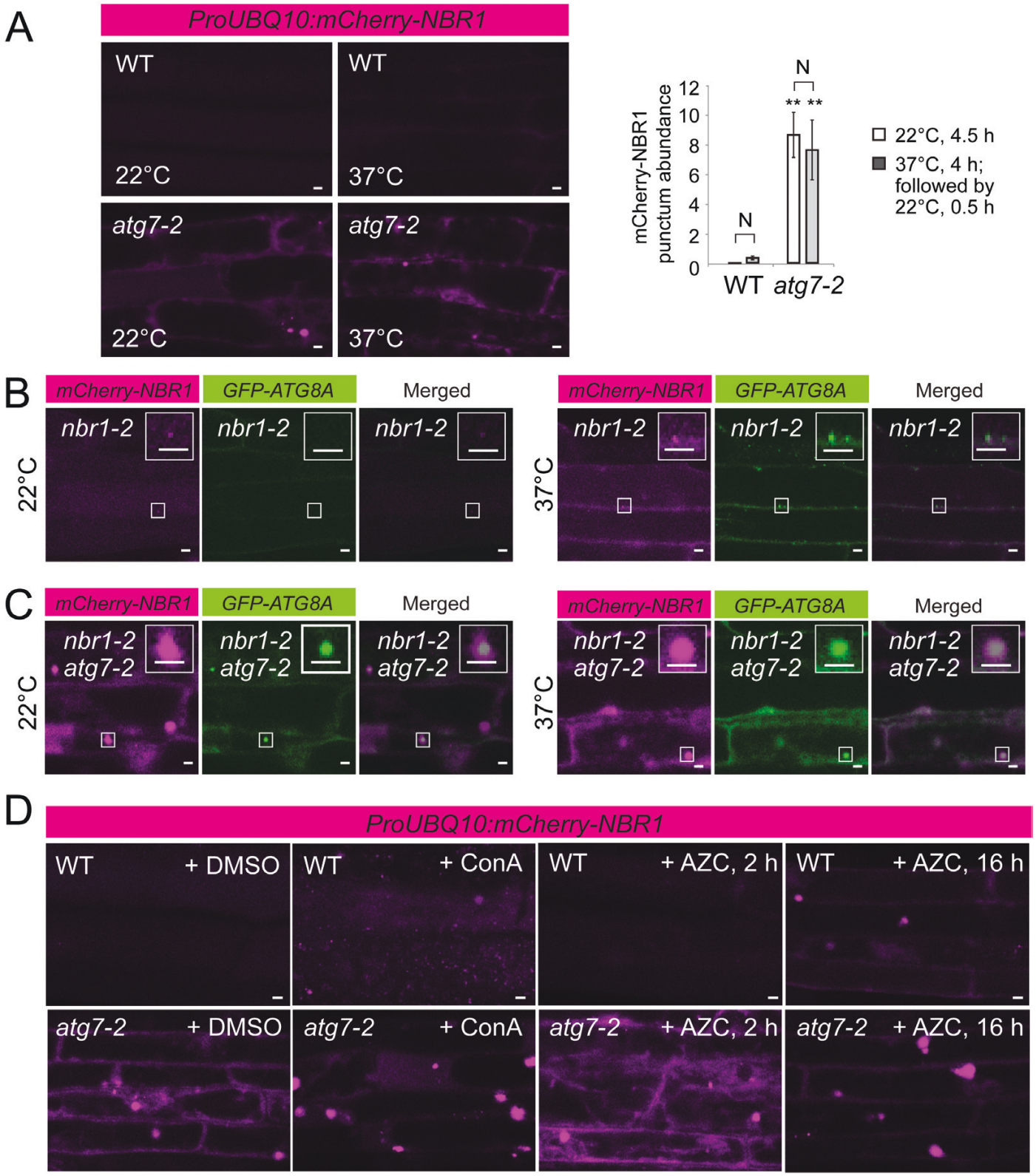

Fig. 4. Autophagy rapidly clears the cytoplasmic puncta decorated with mCherry–NBR1 that form during heat and folding stress. (A) Confocal images of mature root cells expressing *mCherry-NBR1* in wild-type (WT; top) and *atg7-2* (bottom) backgrounds. Seedlings were incubated at 22 °C (control; left) or 37 °C (right) for 4 h, and then recovered at 22 °C for 0.5–1 h prior to observation. The graph on the right shows quantification of mCherry–NBR1 punctum density (number of puncta per 17 424 μm^2) in multiple images represented by those shown on the left. Each column represents the mean ±SE; *n*=15–29 images per sample. Columns marked with asterisks represent treatments or mutants that were significantly different from the control treatment or WT, according to two-way (genotype×treatment) ANOVA followed by Tukey's *post hoc* test. **P<0.01; N, no significant difference. (B, C) Confocal images of mature root cells expressing *mCherry-NBR1* and *GFP-ATG8A* in *nbr1-2* single (B) and *atg7-2 nbr1-2* double (C) mutant backgrounds. Seedlings were incubated at 22 °C (control; left) or 37 °C (right) for 4 h, and then recovered at 22 °C for 0.5–1 h prior to observation. Insets show magnified images. (D) Confocal images of mature root cells expressing *mCherry-NBR1* in WT (top) or *atg7-2* (bottom) backgrounds. Prior to microscopic observation, 9-day-old seedlings were treated with DMSO for 16 h (+ DMSO), 0.5 μM ConA for 16 h (+ ConA), or 2 mM AZC for 2 h or 16 h (+ AZC). Scale bars: 5 μm.

fluorescence was seen, similar to that reported by Svenning *et al.* (2011), which included both a diffuse cytoplasmic pattern and large punctate structures in the cytoplasm in both non-stressed and heat-stressed root cells, and similar to those observed with the GFP–ATG8A reporter (Fig. 4A). Co-localization of mCherry–NBR1 with GFP–ATG8A confirmed that at least some of these puncta contained both reporters, especially after heat shock (Fig. 4B). After a 4-h heat stress of WT roots, 16% (32/195) of mCherry–NBR1 puncta overlapped with GFP–ATG8A signal, whereas only 2% (4/170) overlapped in non-stressed roots (Fig. 4B, insets). Much larger and brighter puncta decorated with both mCherry–NBR1 and GFP–ATG8A accumulated in the *atg7-2* mutant (Fig. 4C, insets), consistent with the increased levels of NBR1 in this background (Fig. 2D).

We also tested how protein misfolding impacted the formation of these NBR1-decorated cytoplasmic foci. Few mCherry–NBR1 puncta were observed in WT roots treated with AZC for 2 h (Fig. 4D; WT, +AZC, 2 h; Supplementary Fig. S4A), but large cytoplasmic puncta decorated with mCherry–NBR1 became abundant after 16 h of treatment (Fig. 4D; WT, +AZC, 16 h). The accumulation of mCherry–NBR1 puncta is not surprising, given a near-complete block in autophagic flux after 16 h of AZC treatment (Fig. 1F). Unlike WT cells exposed to a 4-h heat shock (Figs 3B, 4B), those treated with AZC for 16 h did not show co-localization of GFP–ATG8A with mCherry–NBR1 (Supplementary Fig. S4C), implying that prolonged folding stress somehow prevents GFP–ATG8A from interacting with NBR1-containing aggregates. The number of GFP–ATG8A puncta did not increase during the 16-h exposure to AZC (Supplementary Fig. S4E, F), suggesting that prolonged folding stress impairs an early step in autophagosome biogenesis. By contrast, treatment of *atg7-2* seedlings with AZC significantly increased both the abundance and the size of the GFP–ATG8A puncta (Supplementary Figs S4D–G, S2B, C), indicating that AZC does promote the aggregation of GFP–ATG8A as well as mCherry–NBR1. Taken together, it appears that heat and folding stress induce the accumulation of cytoplasmic structures containing both NBR1 and ATG8 that could reflect cytoplasmic protein condensates awaiting clearance by aggrephagy.

NBR1 helps eliminate a mis-localized mutant form of aggregation-prone FLOURY2

To investigate the overall function(s) of Arabidopsis NBR1 during autophagy, we tested genetically its impact on several selective autophagic routes, including aggrephagy. Using the membrane protein VDAC1 and catalase as markers for mitochondria and peroxisomes, respectively, we found by immunoblot analyses that the *nbr1-2* and *nbr1-3* mutants had little effect on mitophagy and pexophagy (Shibata *et al.*, 2013; Li *et al.*, 2014). Whereas increased levels of both markers were seen in *atg7-2* plants as compared with WT, no such increases were seen in the *nbr1-2* and *nbr1-3* mutants (Fig. 5A). In addition, hypocotyls of WT, *nbr1-3*, and *nbr1-4* seedlings contained similar numbers of peroxisomes, as seen by confocal microscopy with the peroxisomal marker cyan fluorescent protein tagged with the Ser–Lys–Leu tripeptide import signal for peroxisomes (CFP–SKL; Fig. 5B), indicating that NBR1 is not essential for ATG7-dependent pexophagy in hypocotyls following germination (Kim *et al.*, 2013*b*). This result is similar to a recent report by Young *et al.* (2019) also showing that NBR1 is not required for pexophagy in Arabidopsis.

Next, we attempted to provide additional support for NBR1 participating in aggrephagy using an artificial aggregation-prone protein as a substrate. The design of this substrate was based on maize FL2, which is a member of the α-zein family of alcohol-soluble seed storage proteins (Argos *et al.*, 1982; Garratt *et al.*, 1993). FL2 and other α-zeins possess (i) an N-terminal signal peptide (SP) required for co-translational translocation into the ER lumen; (ii) a middle region consisting of 9 or 10 repeat motifs often flanked by multiple glutamines (Fig. 5C); and (iii) an enrichment for hydrophobic residues. During maize endosperm development, FL2 and other zeins are synthesized on the ER and deposited into protein bodies, which are ER subdomains created for storing highly organized protein aggregates with α-zeins located at their center (Lending and Larkins, 1989).

Using the WT *FL2* coding sequence from the maize B73 inbred line, we generated stable Arabidopsis transformants expressing FL2 fused to the N-terminus of GFP in photosynthetic tissues under control of the Rubisco small subunit gene promoter (*ProSSU:FL2-GFP*; Fig. 5C). As expected, we detected GFP fluorescence in an ER-like reticulate pattern in mesophyll cells from Arabidopsis cotyledons (Fig. 5D). To test the possibility that FL2–GFP is targeted to the vacuole via an autophagic pathway involving NBR1, we introgressed the *FL2-GFP* transgene into the *nbr1-4* and *atg7-2* backgrounds, and isolated homozygous mutant seedlings expressing the substrate in the F_2 generation. Upon treatment with ConA, WT and *nbr1-4* cotyledon cells generated autophagic body-like puncta containing FL2–GFP in the vacuole, which were absent in *atg7-2* cells (Fig. 5E), indicating that FL2–GFP was sent to the ER and then targeted for autophagic degradation via a reticulophagy pathway requiring ATG8–PE but not NBR1.

To then exploit FL2 as a cytosolic substrate for aggrephagy, we removed the N-terminal SP sequence (FL2ΔSP) needed for its translation by ER-bound ribosomes, and thus forced its synthesis and accretion in the cytosol. To synthesize high levels of GFP–FL2ΔSP in all cells, it was expressed from the constitutive cauliflower mosaic virus *35S* promoter (*Pro35S:GFP-FL2ΔSP*). When this GFP–FL2ΔSP reporter was analysed by confocal fluorescence microscopy, we failed to observe any diffuse or reticulate fluorescence signals in mesophyll cells of leaves and cotyledons, as had been observed for ER-deposited FL2–GFP (Fig. 5F, and data not shown). Instead, small puncta were occasionally detected within the cytoplasm (indicated by an arrow in Fig. 5F), as expected for protein aggregates. Treatment of the transgenic seedlings with MG132 resulted in stronger accumulation of GFP–FL2ΔSP puncta (Fig. 5G), suggesting that these aggregates are degraded in part by a protein quality control mechanism involving the 26S proteasome.

To test whether NBR1-dependent selective autophagy also mediates the degradation of GFP–FL2ΔSP, we introgressed the *Pro35S:GFP-FL2ΔSP* transgene into the *atg7-2* and *nbr1-2* backgrounds, and analysed cotyledon mesophyll cells by

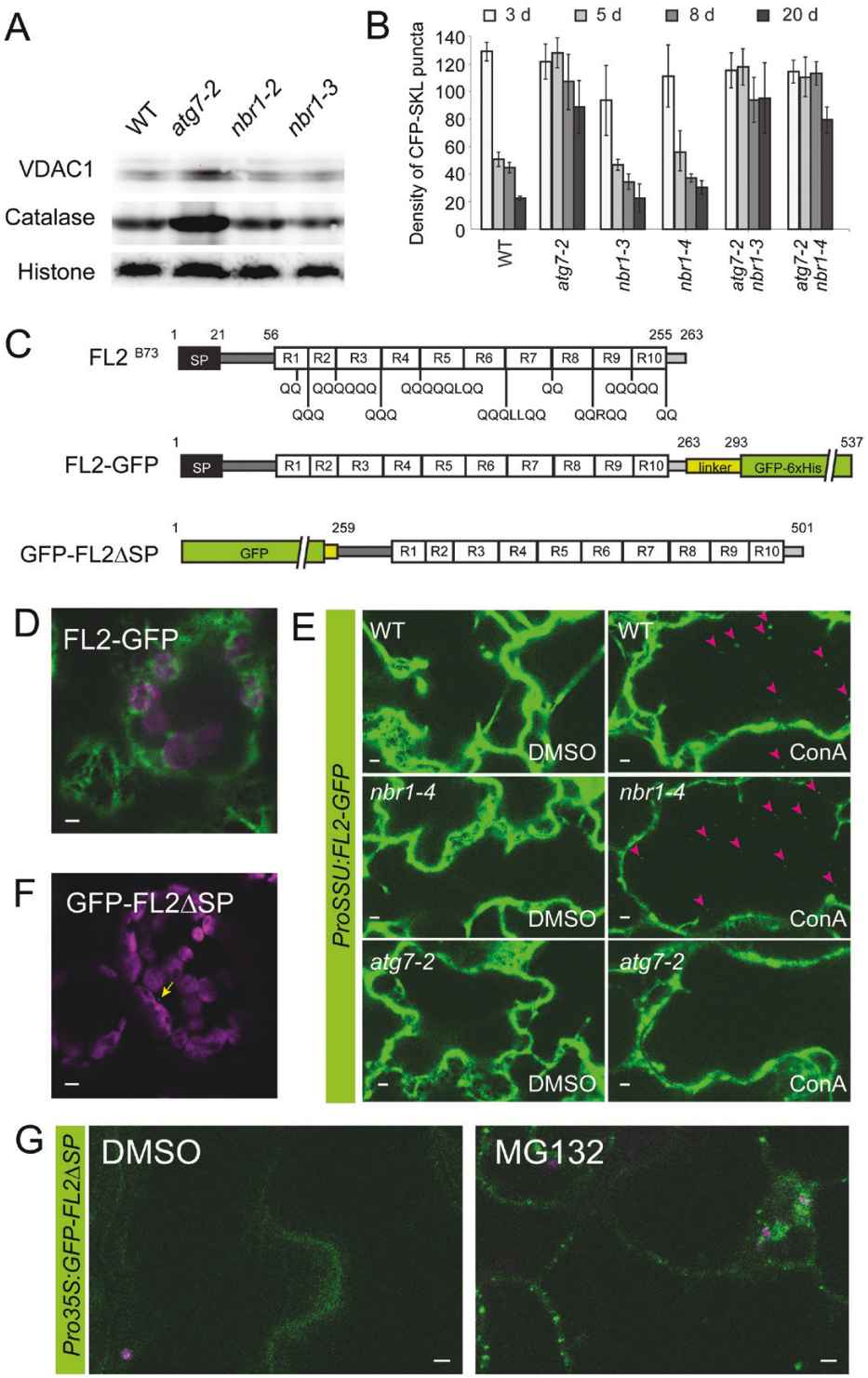

Fig. 5. NBR1 is not required for autophagy of mitochondrial or peroxisomal proteins. (A) Immunoblot of wild-type (WT), *atg7*, or *nbr1* seedling extracts to compare amounts of the mitochondrial and peroxisomal proteins VDAC1 and catalase, respectively. Protein extracts were prepared from the first and second leaves of seedlings grown on solid MS medium for 3 weeks. The anti-histone H3 immunoblot was used to confirm near equal protein loading. (B) Quantification of peroxisome abundance in the hypocotyls of WT, *atg7*, *nbr1*, and *atg7 nbr1* plants. Seedlings expressing the peroxisomal marker CFP–SKL were examined by confocal microscopy at 3, 5, 8, and 20 d after germination. Each column represents the mean ±SD; *n*=3 seedlings. (C) Diagram illustrating primary structures of WT FLOURY2 ($FL2^{B73}$; FL2 derived from the maize B73 inbred line) and its fusion proteins. The N-terminal signal peptide (SP) is shown as a solid box. Ten repeat regions in FL2, designated R1–R10, are indicated by open boxes; glutamine (Q) residues within each repeat are shown. GFP and linker sequences derived from the expression vectors are shown in green and yellow, respectively. Amino acid residues are numbered on the top. (D, F) Confocal fluorescence images of cotyledon mesophyll cells from 9-day-old seedlings expressing FL2–GFP (D) or GFP–FL2ΔSP (F). Chlorophyll autofluorescence is shown in magenta. (E) Confocal fluorescence images of epidermal cells from WT, *atg7-2*, and *nbr1-4* plants expressing FL2–GFP. Seedlings were treated with DMSO or 0.5 μM ConA for 12 h prior to imaging. Magenta arrowheads indicate FL2–GFP puncta resembling autophagic bodies. (G) Confocal fluorescence images of mesophyll cells from plants expressing *Pro35S:GFP-FL2ΔSP*. Nine-day-old seedlings were treated with DMSO or 40 μM MG132 for 2 h prior to microscopic observation of the dissected cotyledons. Scale bars: 5 μm.

confocal fluorescence microscopy (Fig. 6A). When vacuolar proteolysis was inhibited by ConA treatment, GFP–FL2ΔSP puncta could now be observed in the vacuolar region of WT mesophyll cells (Fig. 6A, first row; indicated by arrowheads), implying that aggregation-prone GFP–FL2ΔSP was targeted to the vacuole for degradation. The vacuolar distribution was reduced, while the more peripheral cytoplasmic distribution of GFP–FL2ΔSP puncta was enhanced, in the *atg7* and *nbr1* backgrounds relative to WT, indicating that autophagy and NBR1 are required for this transport (Fig. 6A, B). In support, even ConA treatment failed to enable the appearance of autophagic bodies containing GFP–FL2ΔSP in the *atg7-2* and *nbr1-2* lines. Consistent with these puncta representing aggregated GFP–FL2ΔSP awaiting autophagic clearance, size measurements indicated that they were larger in the *atg7-2* and *nbr1-2* backgrounds, as one might expect if the substrate was allowed to accumulate and coalesce (Fig. 6C). RT-PCR analysis of *GFP-FL2ΔSP* transcripts showed that the increased accumulation of

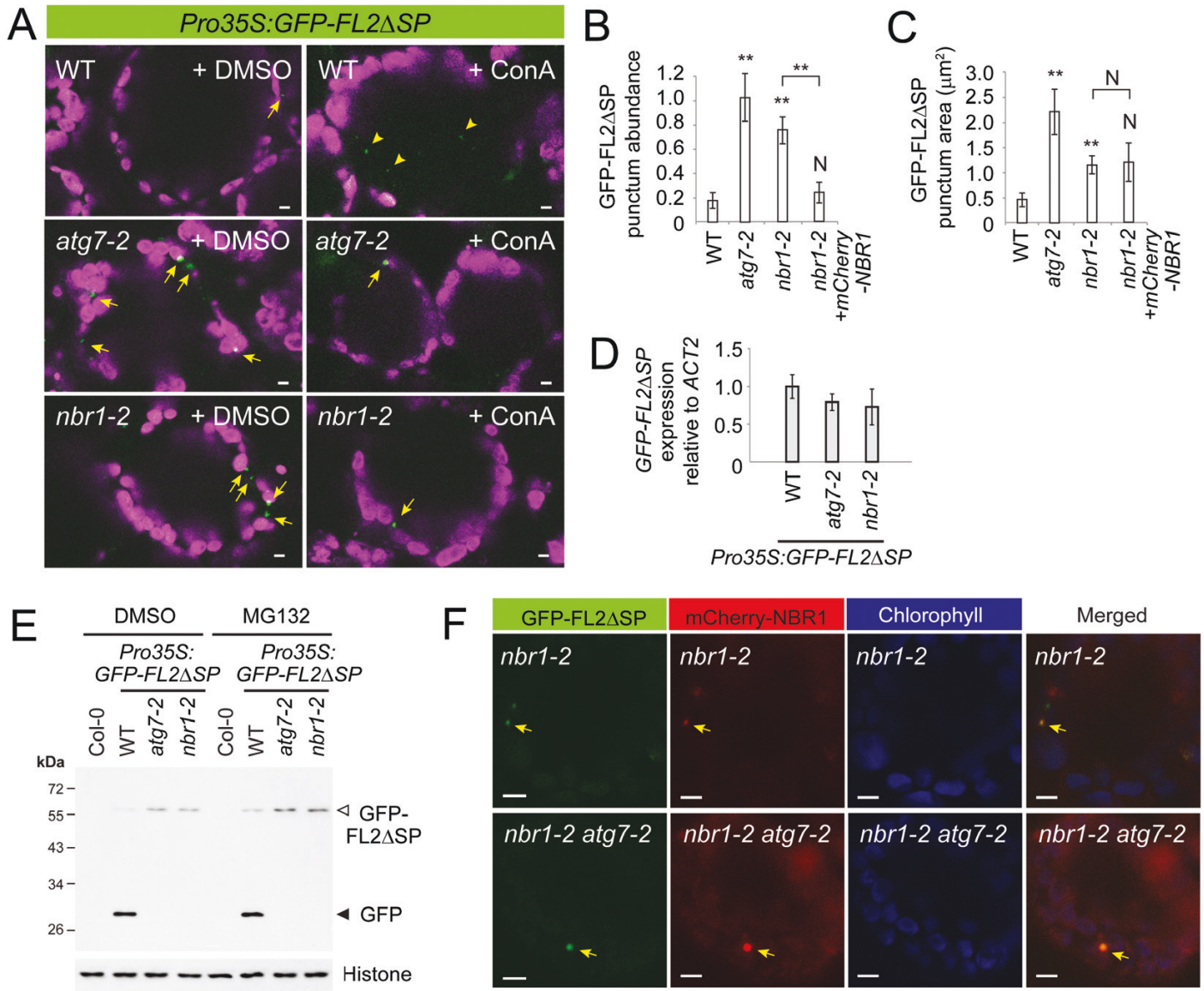

Fig. 6. NBR1 mediates the selective autophagy of GFP–FL2ΔSP. (A) Confocal images of mesophyll cells from wild-type (WT), *atg7-2*, and *nbr1-2* plants expressing *Pro35S:GFP-FL2ΔSP*. Nine-day-old seedlings were treated with DMSO or 0.5 μM ConA for 16 h prior to confocal fluorescence microscopic observation of the dissected cotyledons. Arrows indicate green punctate signal of GFP–FL2ΔSP. Chlorophyll autofluorescence is shown in magenta. (B, C) Quantification of GFP–FL2ΔSP punctum abundance (B) (number of puncta per 8100 μm^2) and dimension (C) in multiple images represented by those shown in (A). Each column represents the mean ±SE; *n*=29–33 images (B), or 6–21 puncta (C) per sample. Columns marked with asterisks (**P<0.01) represent mutants that were significantly different from the WT control, according to Student's *t*-test. N, no significant difference. (D) qRT-PCR analysis to compare levels of *GFP-FL2ΔSP* transcripts in the WT, *atg7-2*, or *nbr1-2* backgrounds. The relative expression of *GFP-FL2ΔSP* was calculated using *ACTIN 2* (*ACT2*) as a reference transcript. Each column represents the mean ±SE; *n*=5 seedling populations. (E) Immunoblot analysis with anti-GFP antibodies showing the steady-state levels of GFP–FL2ΔSP (indicated by the open arrowhead) and its proteolytic cleavage product (solid arrowhead). Protein extracts were prepared from 9-day-old seedlings of the indicated genotypes treated with DMSO (left lanes) or 50 μM MG132 (right lanes) for 2 h. Col-0 indicates a negative control that does not express GFP–FL2ΔSP. The anti-histone H3 immunoblot was used to confirm near equal protein loading. (F) Confocal fluorescence images of mesophyll cells from *nbr1-2* and *atg7-2 nbr1-2* plants expressing both *GFP-FL2ΔSP* and *mCherry-NBR1*. Arrows indicate GFP–FL2ΔSP puncta overlapping with the mCherry–NBR1 fluorescence signal. Chlorophyll auto-fluorescence is shown in blue. Scale bars: 5 μm.

GFP–FL2ΔSP was not caused by its differential expression in the mutant backgrounds (Fig. 6D).

Further analysis by the GFP-cleavage assay supported the targeting of the GFP–FL2ΔSP substrate to autophagy. In WT seedlings expressing GFP–FL2ΔSP, only free GFP was evident by immunoblot analysis (Fig. 6E). However, in the *atg7-2* and *nbr1-2* mutant backgrounds, the fusion was the dominant species, indicating that GFP–FL2ΔSP accumulated only when selective autophagy through NBR1, or the general autophagy machinery through ATG7, was blocked (Fig. 6E). Taken together, we concluded that vacuolar degradation of GFP–FL2ΔSP requires both ATG7 and NBR1.

We next assessed the effect of a 4-h heat shock on the localization of GFP–FL2ΔSP in WT, *atg7-2*, *nbr1-2*, and *atg7-2 nbr1-2* double mutant plants (Supplementary Fig. S5A). Heat shock reduced the abundance of cytoplasmic GFP–FL2ΔSP puncta only slightly in the *nbr1-2* single mutant (Supplementary Fig. S5B). Notably, the *atg7-2 nbr1-2* double mutant did not show additive interactions in terms of punctum abundance in any of the conditions tested (Supplementary Fig. S5B), supporting the notion that *NBR1* and *ATG7* act within the same quality control pathway. Interestingly, the GFP–FL2ΔSP puncta that accumulated in the heat-exposed *atg7-2 nbr1-2* double mutants were noticeably smaller than those in the *atg7-2* single mutant (Supplementary Fig. S5C), suggesting that *NBR1* assists in the expansion of cytoplasmic GFP–FL2ΔSP aggregates. Expression of mCherry–NBR1 in the *nbr1-2* plants restored the number of GFP–FL2ΔSP puncta to WT levels (Fig. 6B), further confirming that NBR1 contributes to the quality control of GFP–FL2ΔSP. In fact, some GFP–FL2ΔSP puncta co-localized with mCherry–NBR1 in both *nbr1-2* single and *atg7-2 nbr1-2* double mutant backgrounds (Fig. 6F), indicating that GFP–FL2ΔSP coalesces with NBR1 in cytoplasmic aggregates prior to autophagy. Taken together, these data support a role for NBR1 as an aggrephagy receptor for GFP–FL2ΔSP.

Arabidopsis NBR1 accumulates when proteasomes are inhibited

Because NBR1 is likely degraded together with aggrephagy cargo (Svenning *et al.*, 2011), we expected that NBR1 biosynthesis would be up-regulated during folding stress and proteasome inhibition to maintain an adequate supply. Consistent with this notion, mammalian p62 is known to hyper-accumulate when 26S proteasomes are blocked by the inhibitors MG132 or bortezomib (Myeku and Figueiredo-Pereira, 2011; Sha *et al.*, 2018). As MG132 treatment also induces a heat shock-like response, including increased transcription of ER chaperones (Bush *et al.*, 1997), it was conceivable that the hyper-accumulation of NBR1 upon exposure to MG132 is a secondary consequence of protein folding stress. This stress would then activate the proteasome-stress regulon that up-regulates a host of genes involved in proteotoxic stress protection, including *NBR1* and loci encoding subunits of the 26S proteasome (Gladman *et al.*, 2016). To validate a specific induction of proteasome synthesis and the folding stress response by MG132, AZC, and/or heat, we monitored the abundance of the mRNA encoding the core 26S proteasome subunit PAA2 (Gladman *et al.*, 2016), and the heat-inducible transcription factor HSF7A or the HSP90 chaperone, both of which are indicative of folding stress (Sugio *et al.*, 2009). We found that a 2-h treatment with MG132 increased *PAA2* transcript levels, but did not greatly induce folding stress, while a 2-h treatment with AZC and heat shock caused folding stress but did not activate *PAA2* expression (Supplementary Fig. S6A).

Subsequently, we tested whether these treatments influenced *NBR1* expression in WT and *atg7-2* seedlings. In both genetic backgrounds, AZC and heat shock did not lead to a significant increase in *NBR1* mRNA (Fig. 7A) and NBR1

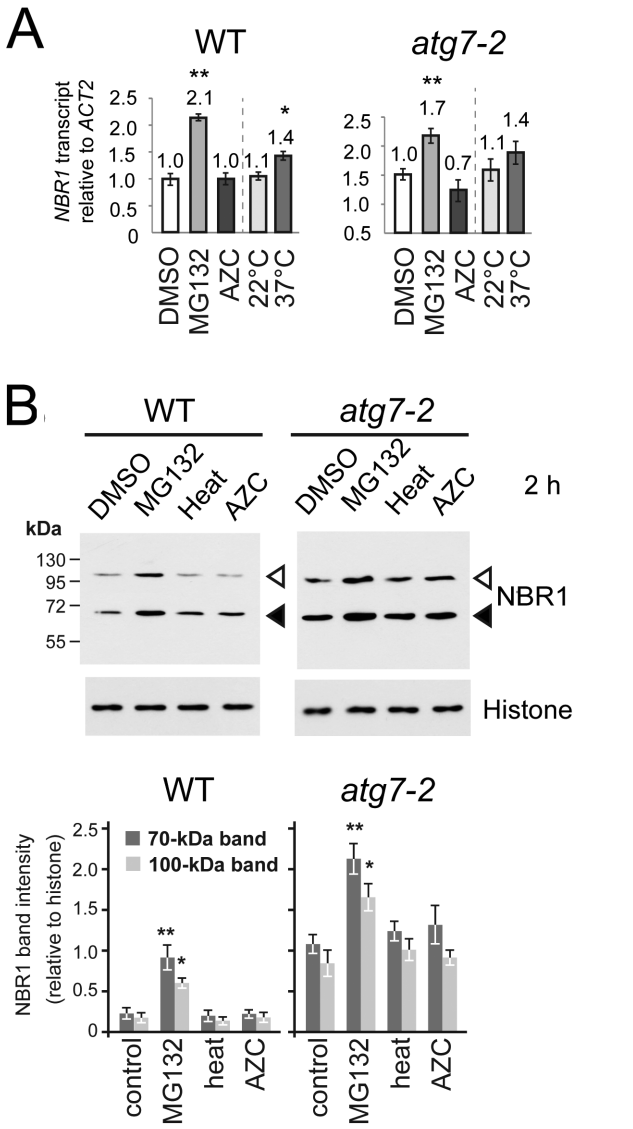

Fig. 7. Proteasome inhibition up-regulates *NBR1* expression in wild-type and *atg7-2* plants. (A, B) *NBR1* transcript levels (A) or immunoblot analysis of NBR1 protein levels (B) in wild-type (WT) and *atg7-2* plants upon elicitation of proteotoxic stress. RNA (A) and protein (B) extracts were prepared from 9-day-old (A) or 7-day-old (B) seedlings treated with DMSO, 40 μM MG132, 2 mM AZC, or a 37 °C heat shock for 2 h. The anti-histone H3 immunoblot was used to confirm near equal protein loading. Each column represents the mean ±SE; *n*=4 (A) or 3 (B) seedling populations. Columns marked with asterisks (*P<0.05; **P<0.01) represent treatment or mutants that were significantly different from their controls, according to Student's *t*-test.

protein levels (Fig. 7B), except for a 1.4-fold increase in *NBR1* mRNA in response to heat shock. By contrast, WT seedlings treated with MG132 hyper-accumulated the *NBR1* transcript (Fig. 7A; Gladman *et al.*, 2016) and NBR1 proteins (Fig. 7B). This change in the *NBR1* transcript level was independent of autophagy, because MG132-treated *atg7-2* seedlings also accumulated higher levels of the *NBR1* transcript (Fig. 7A) and NBR1 proteins (Fig. 7B) when compared with the DMSO-treated control. This autophagy-independent up-regulation of *NBR1* expression is likely important for its aggregation-promoting function. A longer (16-h) treatment did lead to a significant increase in *NBR1* transcript levels under all three conditions (Supplementary Fig. S6B), but hyper-accumulation of the NBR1 proteins was most obvious in seedlings treated with MG132 (Supplementary Fig. S6C). Taken together, these data imply that *NBR1* expression is more rapidly up-regulated by proteasome stress, than by signal(s) generated from misfolded polypeptides.

Discussion

Prior studies showed that plant NBR1 is an autophagy substrate and suggested a conserved role for it in protein aggregation and subsequent aggrephagy (Svenning *et al.*, 2011; Zientara-Rytter *et al.*, 2011, 2014). However, beyond its context in plant immunity (Hafrén *et al.*, 2017, 2018), role(s) of NBR1 in autophagic trafficking and its potential cargo remained to be defined. Here, we demonstrated by several methods that an aggregation-prone substrate, GFP–FL2ΔSP, is degraded in the vacuole via NBR1-mediated autophagy (Fig. 6). Although cytoplasmic GFP–FL2ΔSP was rarely observed in WT cells, its location overlapped with mCherry–NBR1 puncta (Fig. 6F). However, in *atg7* and *nbr1* mutants that would presumably block aggrephagy, substantially more GFP–FL2ΔSP puncta of larger sizes accumulated, as compared with those in WT (Fig. 6A–C). Using the release of free GFP from the GFP–FL2ΔSP reporter as a second assay for autophagy, we found that this release was evident in WT, but was strongly suppressed in *nbr1* and *atg7* backgrounds (Fig. 6E). Finally, our double mutant analysis placed *nbr1* and *atg7* in the same quality control pathway (Supplementary Fig. S5). These data support the hypothesis that NBR1 is an aggrephagy receptor for aggregation-prone and mis-localized proteins, and identifies GFP–FL2ΔSP as a useful marker to track aggrephagy (Fig. 8).

We note that the accumulation of GFP–FL2ΔSP was poor in Arabidopsis despite the use of strong promoters to drive expression. We speculate that GFP–FL2ΔSP so effectively aggregates that it is rapidly degraded through multiple protein quality control pathways, such as the ubiquitin–proteasome system in addition to autophagy (Fig. 8). A key determinant could be the strongly hydrophobic surface of the protein (Neklesa *et al.*, 2011), but mis-localization of GFP–FL2ΔSP in the cytosol might also explain its instability. Specifically, the hydrophobicity of FL2ΔSP and FL2 (whose SP should be removed after ER translocation) is likely similar, but may have different consequences depending on their location in the ER lumen and the cytosol, respectively (Fig. 5D, F). In fact, a morphologically similar aggrephagy of mis-localized proteins was previously described in tobacco suspension culture cells using cytochrome b_5 fused to tetrameric red fluorescent protein (CytB5–RFP) as the substrate. CytB5–RFP was intended to visualize ER membranes but unexpectedly formed cytosolic aggregates, which were shown to be delivered to the vacuole via ATG8-mediated autophagy (Toyooka *et al.*, 2006). It remains to be determined whether this aggrephagy of CytB5-RFP is similarly disrupted by mutations in *NBR1* and core *ATG* genes.

Our genetic data confirmed a role for NBR1 in aggregate formation, which was previously implied by biochemical and cellular studies (Svenning *et al.*, 2011; Zientara-Rytter and Sirko, 2014). The abnormally large cytoplasmic GFP–ATG8A puncta seen in the *atg7-2* mutant were suppressed by the simultaneous absence of *NBR1* (Fig. 3B). Moreover, GFP–FL2ΔSP puncta appeared smaller in the *nbr1-2* single and *nbr1-2 atg7-2* double mutants than in the *atg7-2* single mutant (Fig. 6C; Supplementary Fig. S5C). We speculate that cargo recognition and packaging by NBR1 during aggrephagy relies on its aggregation-promoting ability (Fig. 8A, B), whereas subsequent interaction of NBR1 with ATG8–PE via its AIM assists in the formation of the phagophore around NBR1-positive protein aggregates (Fig. 8A).

We do not yet understand how GFP–FL2ΔSP is recognized by NBR1. Presumably, targets are concentrated in the aggregates through the binding of NBR1 to ubiquitylated proteins via its UBA domain (Svenning *et al.*, 2011). A likely scenario is that GFP–FL2ΔSP undergoes ubiquitylation to mark it for NBR1 recognition. However, we have not yet observed any higher molecular mass versions of GFP–FL2ΔSP by immunoblot analysis with anti-GFP antibodies that could represent ubiquitylated species, even with long exposure times, suggesting that if this modification occurs, it represents a small percentage of the GFP–FL2ΔSP protein pool. In addition, we found that the level of ubiquitylated species did not differ among WT, *atg7*, *nbr1*, and the *atg7 nbr1* double mutants under non-stressed conditions (Supplementary Fig. S7), suggesting that aggrephagy-associated ubiquitylation, if it occurs, would consume only a small portion of the total ubiquitin pool.

Our anti-NBR1 immunoblots detected 70- and 100-kDa species in both WT and *atg7* mutants (Fig. 2D). While the 70-kDa species likely represents the unmodified NBR1 polypeptide, the source of the 100-kDa species is unknown, although genetic evidence indicates that it is derived from NBR1. We speculate that this slower migrating species represents a post-translationally modified form of NBR1 in Arabidopsis, with one possible modification being poly-ubiquitylation. In support, recent studies showed that mammalian p62 is ubiquitylated at its N-terminal and C-terminal regions to regulate its oligomerization and substrate binding, respectively (Pan *et al.*, 2016; Lee *et al.*, 2017). Intriguingly, our previous ubiquitylome studies identified Arabidopsis NBR1 as modified with one or more ubiquitin moieties (Kim *et al.*, 2013*a*).

In the present study, we also investigated how autophagy in Arabidopsis is affected by two forms of proteotoxic stress, namely AZC treatment and heat shock (Fig. 8A). Heat shock has been proposed to induce autophagy in Arabidopsis (Zhou *et al.*,

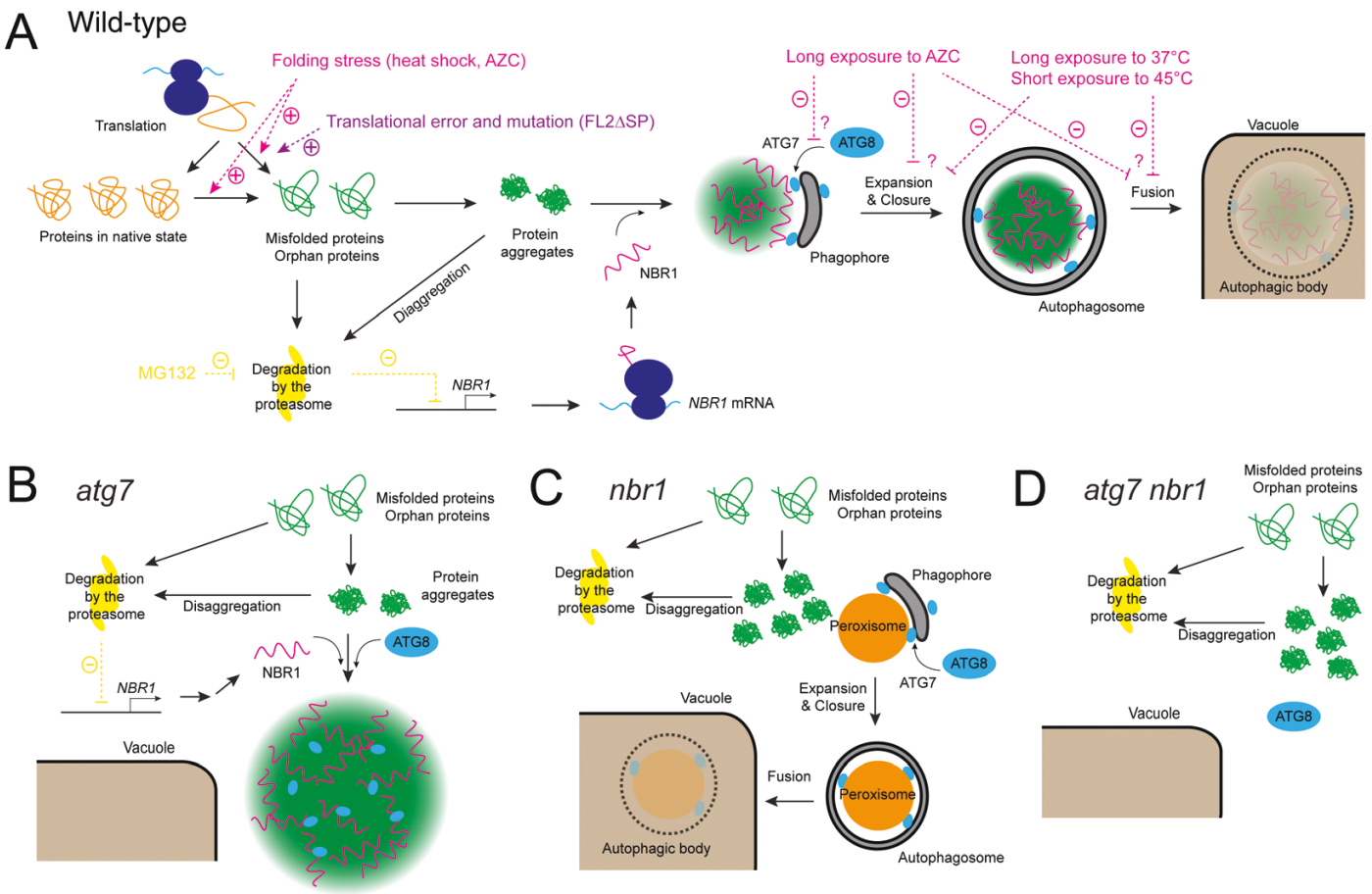

Fig. 8. A model for protein quality control by NBR1-dependent aggrephagy in plant cells. Misfolding of nascent and existing polypeptides might be caused by internal factors (purple arrows with a plus sign), such as translational errors and mutations (e.g. the mutation in FL2ΔSP), and by environments that encourage misfolding (magenta arrows with a plus sign), such as heat shock or drug treatment (e.g. AZC). Misfolded proteins (shown in green) are either degraded by proteasomes or coalesce into aggregates. In wild-type (A) and *atg7* (B) cells, but not in *nbr1* (C) and *atg7 nbr1* (D) cells, these aggregates are sequestered together with NBR1 into a compartment (depicted by the green spheres) specialized for protein quality control. This compartment is cargo for aggrephagy in wild-type cells (A) but not in *atg7* cells (B), in which ATG8 (shown as a light blue oval) cannot be conjugated to the membrane lipid phosphatidylethanolamine and thus either remains in the cytosol or incorporates into an even larger compartment (larger green spheres in B) containing NBR1, non-lipidated ATG8, and aggregation-prone proteins. In wild-type (A) and *nbr1* (C) cells, phagophores develop normally into autophagosomes that are delivered to the lytic vacuole, but aggrephagy is specifically impaired in the *nbr1* mutant (C). Initially, a short exposure to mild heat shock and folding stress (magenta lines with a plus sign) does not impact autophagy. Prolonged folding stress (magenta lines with a minus sign) interferes with a later step in autophagosome dynamics, such as phagophore expansion, closure, and autophagosome fusion with the vacuole. A prolonged exposure to AZC may also inhibit an earlier step (e.g. autophagy induction, phagophore nucleation, or ATG8 conjugation), because heat shock increases the number of autophagic vesicles but treatment with AZC does not. Cells respond to proteasome stress (yellow lines with a minus sign) by increasing *NBR1* transcription, with elevated levels of the NBR1 protein then sequestering protein aggregates that have hyper-accumulated due to impaired proteasome activity. Solid arrows indicate pathways used by proteins, protein aggregates, mRNAs, sequestering compartments, or organelles. Dashed arrows and lines illustrate regulatory relationships, with plus and minus signs representing stimulation and inhibition, respectively.

2013), but the exact timing of its induction was not clarified in detail. Similarly, an increase in autophagic flux was evident in human cell lines during recovery from heat shock (Nivon *et al.*, 2009), but it was not known how autophagic flux is altered during the heat stress period. We showed here that a prolonged exposure to AZC, a proline analog that causes misfolding of nascent polypeptides, strongly inhibits autophagic flux (Fig. 1F), suggesting that proper autophagy can be maintained only for a limited duration without *de novo* protein synthesis and proper protein folding. In addition, we did not detect a significant increase in autophagic flux under a short exposure to heat shock (Fig. 1E). Instead, our data revealed that autophagy is gradually impeded as heat stress persists (Fig. 1; Supplementary Fig. S1). A large fraction of the GFP–ATG8A puncta observed during extended heat stress (Figs 1A, 3B) might represent arrested autophagic vesicles sequestering protein aggregates, because ATG8–PE accumulated in seedlings exposed to a 12-h heat shock, while a combined treatment with ConA did not further increase ATG8–PE levels (Fig. 1D).

We noted that the degree of autophagy inhibition by heat appears to correlate with both duration and temperature. For example, autophagic flux was almost completely blocked by either a 12-h exposure to 37 °C (Fig. 1B) or 2-h exposure to 45 °C (Supplementary Fig. S8A). As Arabidopsis seedlings cannot typically survive a 2-h heat shock at 45 °C (Queitsch *et al.*, 2000), it is advised to avoid such a severe heat stress without prior acclimation at 37 °C when studying autophagy. For the heat-stress experiments, we used seedlings grown in

liquid medium for 9 d, because the hydroponic culture system enabled efficient treatment with ConA and other drugs. Although this system may not be ideal in terms of physiological relevance, seedlings showed a typical response to heat stress in our setting (Supplementary Fig. S6A). When seedlings were exposed to heat, accumulation of cytoplasmic GFP–ATG8A puncta were evident in root cells (Figs 1, 3, 4; Supplementary Figs S3, S4) and cotyledon epidermal cells (Supplementary Fig. S8B), similar to GFP–ATG8A puncta accumulating in the leaf epidermis of plants grown on soil for 4 weeks and exposed to 45 °C for 2 h (Zhou *et al.*, 2013).

It is not clear whether prolonged heat stress impedes autophagy passively (e.g. by heat-inactivation of ATG proteins) or actively (e.g. by down-regulation of ATG proteins). Sedaghatmehr *et al.* (2019) recently reported that autophagic degradation of Arabidopsis heat shock proteins (HSPs) became apparent 2 d after a priming heat shock treatment at 44 °C for 45 min, which was preceded by an adaptive heat shock at 37 °C for 90 min. On one hand, their observations suggest that aggrephagy occurs during a late recovery phase after priming heat shock to possibly erase thermomemory-associated HSPs. Here, we similarly report that autophagic flux was enhanced 12 h after heat shock was relieved (Supplementary Fig. S8C). On the other hand, the data of Sedaghatmehr *et al.* (2019) suggest that HSPs associated with protein aggregates could be protected against futile aggrephagy until HSPs are no longer needed. Similar protective mechanisms were recently described for granulophagy and proteaphagy. Nematode embryos degrade PGL1-containing P granules by autophagy under normal temperatures, whereas a high temperature promotes the formation of larger P granules that are resistant to autophagy (Zhang *et al.*, 2018). Similarly, during fixed carbon starvation, Arabidopsis proteasomes sequester in proteasome storage granules to avoid autophagic clearance (Marshall and Vierstra, 2018*b*). As autophagic flux is not altered during an early recovery phase (up to 4 h) after 37 °C heat shock (Supplementary Fig. S8D), future investigation of mechanisms for potentially down-regulating autophagy may focus on the early recovery phase.

In summary, our data collectively support a role for NBR1 in aggrephagy as a receptor for cytosolic aggregates (Fig. 8) and provide a novel synthetic substrate to track its activity. Whereas general autophagy and other types of selective autophagy were not affected by eliminating *NBR1*, it remains possible that NBR1 still participates in a non-essential manner. Although our study implicates NBR1 in promoting aggregate formation, how NBR1 recognizes appropriate targets in plants, and whether ubiquitylation of targets is involved in this process, remain to be investigated. Cooperation of NBR1-mediated aggrephagy with the ubiquitin–proteasome system and (co) chaperones is an interesting topic for future research (Yoon and Chung, 2019; McLoughlin *et al.*, 2019).

Supplementary data

Supplementary data are available at *JXB* online.

Fig. S1. Analysis of autophagy markers in Arabidopsis seedlings exposed to heat stress and nitrogen starvation.

Fig. S2. NBR1 plays a minor role in general autophagic flux.

Fig. S3. Analysis of autophagy markers in *nbr1-4* seedlings after heat stress.

Fig. S4. Autophagy marker analysis of root cells upon protein folding stress.

Fig. S5. NBR1 is essential for the ATG7-dependent selective autophagy of GFP–FL2ΔSP.

Fig. S6. Autophagy-dependent and -independent effect of proteotoxic stress on *NBR1* expression.

Fig. S7. Levels of ubiquitylated proteins in *nbr1* mutants are indistinguishable from wild-type.

Fig. S8. Analysis of autophagy markers in Arabidopsis cells following recovery from heat stress.

Table S1. Oligonucleotide primers used in this study.

Acknowledgements

This work was supported by a grant from the National Research Foundation of Korea (NRF-2017R1A2B4002335) to TC and by grants from the US National Science Foundation - Plant Genome Research Program (IOS-1339325 and IOS-1840687), and the National Institutes of Health; National Institute of General Medical Science (RO1-GM124452) to RDV.

References

Argos P, Pedersen K, Marks MD, Larkins BA. 1982. A structural model for maize zein proteins. The Journal of Biological Chemistry **257**, 9984–9990.

Avin-Wittenberg T. 2019. Autophagy and its role in plant abiotic stress management. Plant, Cell & Environment **42**, 1045–1053.

Avin-Wittenberg T, Baluska F, Bozhkov PV, *et al*. 2018. Autophagy-related approaches for improving nutrient use efficiency and crop yield protection. Journal of Experimental Botany **69**, 1335–1353.

Bjørkøy G, Lamark T, Brech A, Outzen H, Perander M, Overvatn A, Stenmark H, Johansen T. 2005. p62/SQSTM1 forms protein aggregates degraded by autophagy and has a protective effect on huntingtin-induced cell death. The Journal of Cell Biology **171**, 603–614.

Bush KT, Goldberg AL, Nigam SK. 1997. Proteasome inhibition leads to a heat-shock response, induction of endoplasmic reticulum chaperones, and thermotolerance. The Journal of Biological Chemistry **272**, 9086–9092.

Chung T, Phillips AR, Vierstra RD. 2010. ATG8 lipidation and ATG8-mediated autophagy in Arabidopsis require ATG12 expressed from the differentially controlled *ATG12A* and *ATG12B* loci. The Plant Journal **62**, 483–493.

Clough SJ, Bent AF. 1998. Floral dip: a simplified method for *Agrobacterium*-mediated transformation of *Arabidopsis thaliana*. The Plant Journal **16**, 735–743.

Curtis MD, Grossniklaus U. 2003. A Gateway cloning vector set for high-throughput functional analysis of genes *in planta*. Plant Physiology **133**, 462–469.

Dagdas YF, Belhaj K, Maqbool A, *et al*. 2016. An effector of the Irish potato famine pathogen antagonizes a host autophagy cargo receptor. eLife **5**, e10856.

Dagdas YF, Pandey P, Tumtas Y, *et al*. 2018. Host autophagy machinery is diverted to the pathogen interface to mediate focal defense responses against the Irish potato famine pathogen. eLife **7**, e37476.

Duttler S, Pechmann S, Frydman J. 2013. Principles of cotranslational ubiquitination and quality control at the ribosome. Molecular Cell **50**, 379–393.

Garratt R, Oliva G, Caracelli I, Leite A, Arruda P. 1993. Studies of the zein-like α-prolamins based on an analysis of amino acid sequences: implications for their evolution and three-dimensional structure. Proteins **15**, 88–99.

Gladman NP, Marshall RS, Lee KH, Vierstra RD. 2016. The proteasome stress regulon is controlled by a pair of NAC transcription factors in *Arabidopsis*. The Plant Cell **28**, 1279–1296.

Hafrén A, Macia JL, Love AJ, Milner JJ, Drucker M, Hofius D. 2017. Selective autophagy limits cauliflower mosaic virus infection by NBR1-mediated targeting of viral capsid protein and particles. Proceedings of the National Academy of Sciences, USA **114**, 2026–2035.

Hafrén A, Üstün S, Hochmuth A, Svenning S, Johansen T, Hofius D. 2018. Turnip mosaic virus counteracts selective autophagy of the viral silencing suppressor HCpro. Plant Physiology **176**, 649–662.

Harper JW, Bennett EJ. 2016. Proteome complexity and the forces that drive proteome imbalance. Nature **537**, 328–338.

Haxim Y, Ismayil A, Jia Q, *et al*. 2017. Autophagy functions as an antiviral mechanism against geminiviruses in plants. eLife **6**, e23897.

Kang S, Shin KD, Kim JH, Chung T. 2018. Autophagy-related (ATG) 11, ATG9 and the phosphatidylinositol 3-kinase control ATG2-mediated formation of autophagosomes in Arabidopsis. Plant Cell Reports **37**, 653–664.

Kim DY, Scalf M, Smith LM, Vierstra RD. 2013*a*. Advanced proteomic analyses yield a deep catalog of ubiquitylation targets in *Arabidopsis*. The Plant Cell **25**, 1523–1540.

Kim J, Lee H, Lee HN, Kim SH, Shin KD, Chung T. 2013*b*. Autophagy-related proteins are required for degradation of peroxisomes in *Arabidopsis* hypocotyls during seedling growth. The Plant Cell **25**, 4956–4966.

Komatsu M, Waguri S, Koike M, *et al*. 2007. Homeostatic levels of p62 control cytoplasmic inclusion body formation in autophagy-deficient mice. Cell **131**, 1149–1163.

Lee Y, Chou TF, Pittman SK, Keith AL, Razani B, Weihl CC. 2017. Keap1/Cullin3 modulates p62/SQSTM1 activity via UBA domain ubiquitination. Cell Reports **19**, 188–202.

Lending CR, Larkins BA. 1989. Changes in the zein composition of protein bodies during maize endosperm development. The Plant Cell **1**, 1011–1023.

Li F, Chung T, Vierstra RD. 2014. AUTOPHAGY-RELATED11 plays a critical role in general autophagy- and senescence-induced mitophagy in *Arabidopsis*. The Plant Cell **26**, 788–807.

Liu Y, Burgos JS, Deng Y, Srivastava R, Howell SH, Bassham DC. 2012. Degradation of the endoplasmic reticulum by autophagy during endoplasmic reticulum stress in *Arabidopsis*. The Plant Cell **24**, 4635–4651.

Livak KJ, Schmittgen TD. 2001. Analysis of relative gene expression data using real-time quantitative PCR and the $2^{-\Delta\Delta C(T)}$ method. Methods **25**, 402–408.

Marshall RS, Hua Z, Mali S, McLoughlin F, Vierstra RD. 2019. ATG8-binding UIM proteins define a new class of autophagy adaptors and receptors. Cell **177**, 766–781.

Marshall RS, Li F, Gemperline DC, Book AJ, Vierstra RD. 2015. Autophagic degradation of the 26S proteasome is mediated by the dual ATG8/ubiquitin receptor RPN10 in *Arabidopsis*. Molecular Cell **58**, 1053–1066.

Marshall RS, Vierstra RD. 2018*a*. Autophagy: the master of bulk and selective recycling. Annual Review of Plant Biology **69**, 173–208.

Marshall RS, Vierstra RD. 2018*b*. Proteasome storage granules protect proteasomes from autophagic degradation upon carbon starvation. eLife **7**, e34532.

McLoughlin F, Kim M, Marshall RS, Vierstra RD, Vierling E. 2019. HSP101 interacts with the proteasome and promotes the clearance of ubiquitylated protein aggregates. Plant Physiology **180**, 1829–1847.

Mizushima N, Yoshimori T, Levine B. 2010. Methods in mammalian autophagy research. Cell **140**, 313–326.

Mogk A, Bukau B, Kampinga HH. 2018. Cellular handling of protein aggregates by disaggregation machines. Molecular Cell **69**, 214–226.

Myeku N, Figueiredo-Pereira ME. 2011. Dynamics of the degradation of ubiquitinated proteins by proteasomes and autophagy: association with sequestosome 1/p62. The Journal of Biological Chemistry **286**, 22426–22440.

Neklesa TK, Tae HS, Schneekloth AR, Stulberg MJ, Corson TW, Sundberg TB, Raina K, Holley SA, Crews CM. 2011. Small-molecule hydrophobic tagging-induced degradation of HaloTag fusion proteins. Nature Chemical Biology **7**, 538–543.

Nivon M, Richet E, Codogno P, Arrigo AP, Kretz-Remy C. 2009. Autophagy activation by NFκB is essential for cell survival after heat shock. Autophagy **5**, 766–783.

Noda NN, Kumeta H, Nakatogawa H, Satoo K, Adachi W, Ishii J, Fujioka Y, Ohsumi Y, Inagaki F. 2008. Structural basis of target recognition by Atg8/LC3 during selective autophagy. Genes to Cells **13**, 1211–1218.

Pan JA, Sun Y, Jiang YP, *et al*. 2016. TRIM21 ubiquitylates SQSTM1/p62 and suppresses protein sequestration to regulate redox homeostasis. Molecular Cell **61**, 720–733.

Pankiv S, Clausen TH, Lamark T, Brech A, Bruun JA, Outzen H, Øvervatn A, Bjørkøy G, Johansen T. 2007. p62/SQSTM1 binds directly to Atg8/LC3 to facilitate degradation of ubiquitinated protein aggregates by autophagy. The Journal of Biological Chemistry **282**, 24131–24145.

Queitsch C, Hong SW, Vierling E, Lindquist S. 2000. Heat shock protein 101 plays a crucial role in thermotolerance in *Arabidopsis*. The Plant Cell **12**, 479–492.

Sedaghatmehr M, Thirumalaikumar VP, Kamranfar I, Marmagne A, Masclaux-Daubresse C, Balazadeh S. 2019. A regulatory role of autophagy for resetting the memory of heat stress in plants. Plant, Cell & Environment **42**, 1054–1064.

Sha Z, Schnell HM, Ruoff K, Goldberg A. 2018. Rapid induction of p62 and GABARAPL1 upon proteasome inhibition promotes survival before autophagy activation. The Journal of Cell Biology **217**, 1757–1776.

Shibata M, Oikawa K, Yoshimoto K, Kondo M, Mano S, Yamada K, Hayashi M, Sakamoto W, Ohsumi Y, Nishimura M. 2013. Highly oxidized peroxisomes are selectively degraded via autophagy in *Arabidopsis*. The Plant Cell **25**, 4967–4983.

Shin KD, Lee HN, Chung T. 2014. A revised assay for monitoring autophagic flux in *Arabidopsis thaliana* reveals involvement of AUTOPHAGY-RELATED9 in autophagy. Molecules and Cells **37**, 399–405.

Sláviková S, Shy G, Yao Y, Glozman R, Levanony H, Pietrokovski S, Elazar Z, Galili G. 2005. The autophagy-associated *Atg8* gene family operates both under favourable growth conditions and under starvation stresses in *Arabidopsis* plants. Journal of Experimental Botany **56**, 2839–2849.

Sugio A, Dreos R, Aparicio F, Maule AJ. 2009. The cytosolic protein response as a subcomponent of the wider heat shock response in *Arabidopsis*. The Plant Cell **21**, 642–654.

Suttangkakul A, Li F, Chung T, Vierstra RD. 2011. The ATG1/ATG13 protein kinase complex is both a regulator and a target of autophagic recycling in *Arabidopsis*. The Plant Cell **23**, 3761–3779.

Svenning S, Lamark T, Krause K, Johansen T. 2011. Plant NBR1 is a selective autophagy substrate and a functional hybrid of the mammalian autophagic adapters NBR1 and p62/SQSTM1. Autophagy **7**, 993–1010.

Thompson AR, Doelling JH, Suttangkakul A, Vierstra RD. 2005. Autophagic nutrient recycling in Arabidopsis directed by the ATG8 and ATG12 conjugation pathways. Plant Physiology **138**, 2097–2110.

Toyooka K, Moriyasu Y, Goto Y, Takeuchi M, Fukuda H, Matsuoka K. 2006. Protein aggregates are transported to vacuoles by a macroautophagic mechanism in nutrient-starved plant cells. Autophagy **2**, 96–106.

Trotter EW, Kao CM, Berenfeld L, Botstein D, Petsko GA, Gray JV. 2002. Misfolded proteins are competent to mediate a subset of the responses to heat shock in *Saccharomyces cerevisiae*. The Journal of Biological Chemistry **277**, 44817–44825.

Üstün S, Hafrén A, Liu Q, Marshall RS, Minina EA, Bozhkov PV, Vierstra RD, Hofius D. 2018. Bacteria exploit autophagy for proteasome degradation and enhanced virulence in plants. The Plant Cell **30**, 668–685.

Wang F, Durfee LA, Huibregtse JM. 2013. A cotranslational ubiquitination pathway for quality control of misfolded proteins. Molecular Cell **50**, 368–378.

Wurzer B, Zaffagnini G, Fracchiolla D, Turco E, Abert C, Romanov J, Martens S. 2015. Oligomerization of p62 allows for selection of ubiquitinated cargo and isolation membrane during selective autophagy. eLife **4**, e08941.

Yang X, Srivastava R, Howell SH, Bassham DC. 2016. Activation of autophagy by unfolded proteins during endoplasmic reticulum stress. The Plant Journal **85**, 83–95.

Yoon SH, Chung T. 2019. Protein and RNA quality control by autophagy in plant cells. Molecules and Cells **42**, 285–291.

Yoshimoto K, Hanaoka H, Sato S, Kato T, Tabata S, Noda T, Ohsumi Y. 2004. Processing of ATG8s, ubiquitin-like proteins, and their deconjugation by ATG4s are essential for plant autophagy. The Plant Cell **16**, 2967–2983.

Young PG, Passalacqua MJ, Chappell K, Llinas RJ, Bartel B. 2019. A facile forward-genetic screen for *Arabidopsis* autophagy mutants reveals twenty-one loss-of-function mutations disrupting six *ATG* genes. Autophagy **15**, 941–959.

Zhang G, Wang Z, Du Z, Zhang H. 2018. mTOR regulates phase separation of PGL granules to modulate their autophagic degradation. Cell **174**, 1492–1506.e22.

Zhou J, Wang J, Cheng Y, Chi YJ, Fan B, Yu JQ, Chen Z. 2013. NBR1-mediated selective autophagy targets insoluble ubiquitinated protein aggregates in plant stress responses. PLoS Genetics **9**, e1003196.

Zientara-Rytter K, Lukomska J, Moniuszko G, Gwozdecki R, Surowiecki P, Lewandowska M, Liszewska F, Wawrzyńska A, Sirko A. 2011. Identification and functional analysis of Joka2, a tobacco member of the family of selective autophagy cargo receptors. Autophagy **7**, 1145–1158.

Zientara-Rytter K, Sirko A. 2014. Significant role of PB1 and UBA domains in multimerization of Joka2, a selective autophagy cargo receptor from tobacco. Frontiers in Plant Science **5**, 13.